UCLA
UCLA Electronic Theses and Dissertations

Title

Heterogeneous Functional Organization of Somatostatin- and Dopamine-containing Wide-field Amacrine Cells in Mouse Retina

Permalink

https://escholarship.org/uc/item/74b76099

Author

Vuong, Helen Elaine

Publication Date

2012

Peer reviewed|Thesis/dissertation

eScholarship.org Powered by the California Digital Library
University of California

UNIVERSITY OF CALIFORNIA
Los Angeles

Heterogeneous functional organization of somatostatin- and dopamine-containing wide-field amacrine cells in mouse retina

A thesis submitted in partial satisfaction of the requirements for the degree Master of Science in Physiological Science

By

Helen Elaine Vuong

2012

© Copyright by

Helen Elaine Vuong

2012

ABSTRACT OF THE THESIS

Heterogeneous functional organization of somatostatin- and dopamine-containing wide-field amacrine cells in mouse retina

By

Helen Elaine Vuong
Master of Science in Physiological Science
2012
Professor Nicholas C. Brecha, Co-chair
Professor Stephanie A. White, Co-chair

In the retina, somatostatin (SRIF) is an inhibitory neuropeptide that influences multiple cell types, including bipolar, amacrine and ganglion cells. SRIF is reported to have multiple cellular actions including modulation of the release of dopamine (DA) from tyrosine hydroxylase (TH)-containing amacrine cells; however, the cellular basis of this interaction is unknown. Using immunohistochemistry I showed SRIF- and TH-containing wide-field amacrine cells co-stratify in the OFF sublamina of the inner plexiform layer (IPL) adjacent to the inner nuclear layer (INL). These processes form a dense network, which co-ramify and make numerous contacts along their processes and at varicosities. SRIF- and TH-immunoreactive (IR) cell bodies and processes also contain GABA and vesicular GABA transporter (VGAT) immunoreactivity, and express the $GABA_A$ α3 receptor subunit. TH-IR cells also express the SRIF receptor subtype 2A (sst_{2A}) and SRIF-IR cells express the D1 receptor. Calcium imaging recordings of Fluo-4 labeled TH-red fluorescent protein (TH-RFP) processes exhibited a ~40% decrease in fluorescent intensity following 60 mM [K^+] depolarization in the presence of SRIF (100nM-100 μM) and L054264 (1-10μM), a selective sst_{2A} agonist. These findings suggest a reciprocal relationship between these two amacrine cell types mediated by both feedback and feed forward actions. SRIF amacrine cells act at TH-containing amacrine cells by a paracrine mechanism at sst_{2A}, as well as directly

at $GABA_A$ receptors. TH amacrine cells likely act at SRIF-containing amacrine cells at D1 and $GABA_A$ receptors. This retinal microcircuit defines a novel modulatory relationship for SRIF and demonstrates its broad influence on multiple visual processes.

The thesis of Helen Elaine Vuong is approved.

Dwayne De Angelo Simmons

Stephanie A. White, Committee Co-chair

Nicholas C. Brecha, Committee Co-chair

University of California, Los Angeles

2012

DEDICATION

I am forever indebted to my family, friends and colleagues who have supported and guided me through the process of achieving this Master of Science degree. I would like to dedicate this thesis to them and their love.

My parents, Dianna Ly and Vinh Hon Vuong are the most supportive, encouraging and loving parents that anyone could ever ask for. I especially appreciate all the delicious meals that my mom cooks for me. I don't think studying would have been as productive without the endless supplies of snacks that she would pack for me! My mom is my rock, if I ever needed advice she would be the voice of reason and I know she always be my biggest supporter. My dad is just that person that I know that no matter what I do in life, he would be the first one to say "Go for it!"

My dearest brothers: Tony Ly and Alexander Hon Vuong. My older brother Tony always picked on me when we were younger, but what older brother doesn't pick on their younger siblings. Today I know that this big bully will have my back and stand up for me in any situation. Alex, my younger brother, best friend, and twin (born three years later). I have learned so much from Alex, though he is younger, he has a mature and responsible mindset. Alex has taught me to live, love, and laugh. When everything seems to be going from bad to worse, Alex takes an optimistic approach and makes me realize that I'm fine and things will get better.

My best friend Jennifer Nhu Huynh. I know I can be a handful sometimes, but Jennifer will always put up with me. She knows how to make me angry, cry, and laugh. We annoy each other, but at the end of the day she is the sister that I always wish I had. I know that no matter where life takes us in the future we will always be best friends and that we are each other's loudest cheerleaders.

I can't forget everyone that has been in the Brecha Lab in the past three years that have been my best buddies. Helen Lee Kornmann ("Big Helen") you are such a sunshine to a long day of lab. Allison

Michelle Sargoy (“Sargoy”) you are my coffee, jokester, calcium imaging and best lab buddy. I thank both of you for always being the best lab buddies in the world!

Thank you guys for everything, I love you guys!

I would like to send a special thanks to Drs. Luis Perez de Sevilla Muller, Iona Raymond, Arlene Hirano, Steve Barnes and Salvatore Stella, Jr., for their helpful discussions regarding the experimental design and comments on the manuscript.

TABLE OF CONTENTS

Chapter 1. Introduction

I. The Retina

The retina is regarded as an extension of the central nervous system, originating as an outgrowth of the developing brain. All vertebrate retinas are divided into three cell body layers and two synaptic layers, and composed of five basic retinal cell types, excluding glial cells: photoreceptors, horizontal cells, bipolar cells, amacrine cells, and ganglion cells (Fig. 1.1).

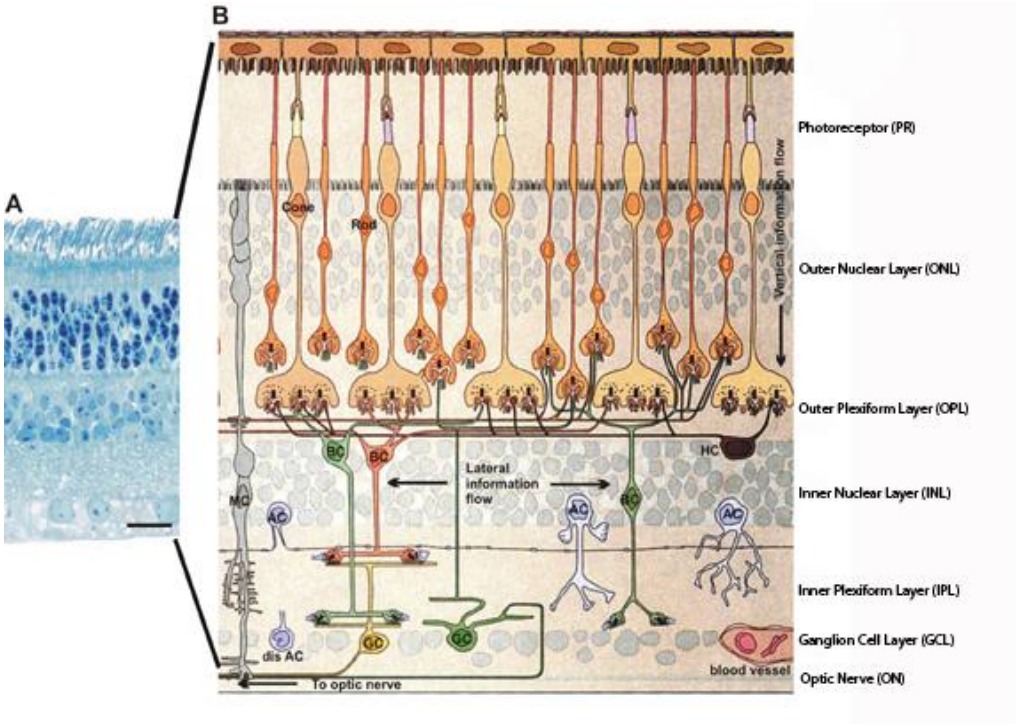

Figure 1.1. Cross section and schematic of the retina. (Modified from Universitat der Bundeswehr Munchen. http://www.anatomy.unimelb.edu.au/researchlabs/rees/images/ retina.jpg)

Light enters the eye and travels past each layer of the retina before the initial processing of photons, which occur at the outer segment of the photoreceptors. Photoreceptor cell bodies rest in the outer nuclear layer (ONL). Photoreceptor terminals make synaptic connections in the outer plexiform layer (OPL) with horizontal cell endings and bipolar cell dendrites, forming the 'synaptic triad'. Located anterior to the OPL is the inner nuclear layer (INL), which consists of horizontal, bipolar, and amacrine cell somatas.

Entering into the inner retina, bipolar and amacrine cells make synaptic connections with ganglion cells in the inner plexiform layer (IPL). The ganglion cell somatas rest in the ganglion cell layer (GCL) and its axons form the nerve fiber layer (NFL) and the bundle of ganglion cell axons leave the eye forming the optic nerve, optic chiasm and optic tract. Using its layered feedfoward and feedback properties of both electrical and chemical signals, the retina is able to process and refine visual information and subsequently relay the neural signals to the cortical vision processing centers.

II. Amacrine Cells

Located in the inner half of the retina, amacrine cells form the most heterogeneous retinal cell type, with more than 30 different subtypes (Badea and Nathans, 2004) categorized based on anatomical and neurochemical phenotypes (Fig. 1.2).

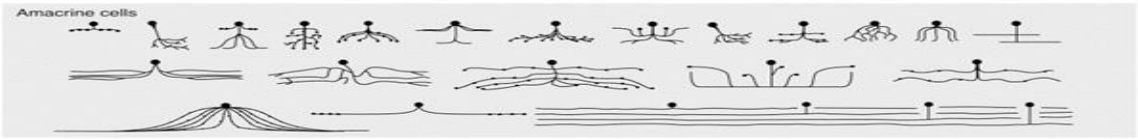

Figure 1.1. Morphological traces of 21 different amacrine cell subtypes. (Adopted from Richard H. Masland, 2011)

Although we know little about the functional properties of amacrine cells, relative to its many different subtypes, recent studies have made great strides in defining the functional organization of certain amacrine cells. In general, amacrine cells form lateral processes that receive synaptic input from bipolar cells and other amacrine cells. The starburst amacrine cells participate in direction-selective retinal circuits by inhibition on to directional selective ganglion cells. Other forms of amacrine cells likely play modulatory roles, allowing adjustment of sensitivity for photopic and scotopic vision. In particular, recent studies on AII amacrine cells suggest that these cells are responsible for translating information from rod bipolar cells to cone bipolar cells, which subsequently convey that information to the respective ganglion

cells through gap-junction coupling (Mills and Massey, 1995). Of particular interest here are the wide-field amacrine cells (WFAC), which morphologically exhibit extensive dendritic arborizations. The WFACs are thought to contribute to inhibitory surrounds by feedback on to bipolar cells, and feedfoward on to ganglion cells (Heflin and Cook, 2007; Bin and Masland, 2006). Most amacrine cells are inhibitory and primarily contain either GABA or glycine as neurotransmitters. However, a subset of amacrine cells also contains other neuromodulators or neuropeptides such as VIP, NPY, somatostatin, and dopamine.

i. Wide-field amacrine cells

Frequently, amacrine cells are characterized by their dendritic tree size; more specifically, narrow-field amacrine cells (<125μm) have small dendritic arbors (MacNiel and Masland, 1998) and express glycine (Menger et al. 1998, Wassle et al., 2009), whereas the less numerous (Masland, 2011) medium- and wide-field amacrine cells are made up of large dendritic arbors that spread laterally, covering up to 1mm (Dedek et al., 2011) and express GABA (Majumdar et al, 2009) (Fig. 1.3).

Among the ~17 different types of medium and wide-field amacrine cells (Badea and Nathans, 2004, Lin and Masland 2006, Perez De Sevilla Muller et al. 2007) there are two which express other neurotransmitters or neuropeptides aside from GABA, in particular the somatostatin- and dopamine-containing amacrine cells. These two wide-field amacrine cells have been individually studied and detailed in their modulation of other retinal cells; however, their precise interactive modulation of each other remains unknown. The combination of anatomical and neurochemical differences allow for defining of the morphological and functional correlations between the two amacrine cells.

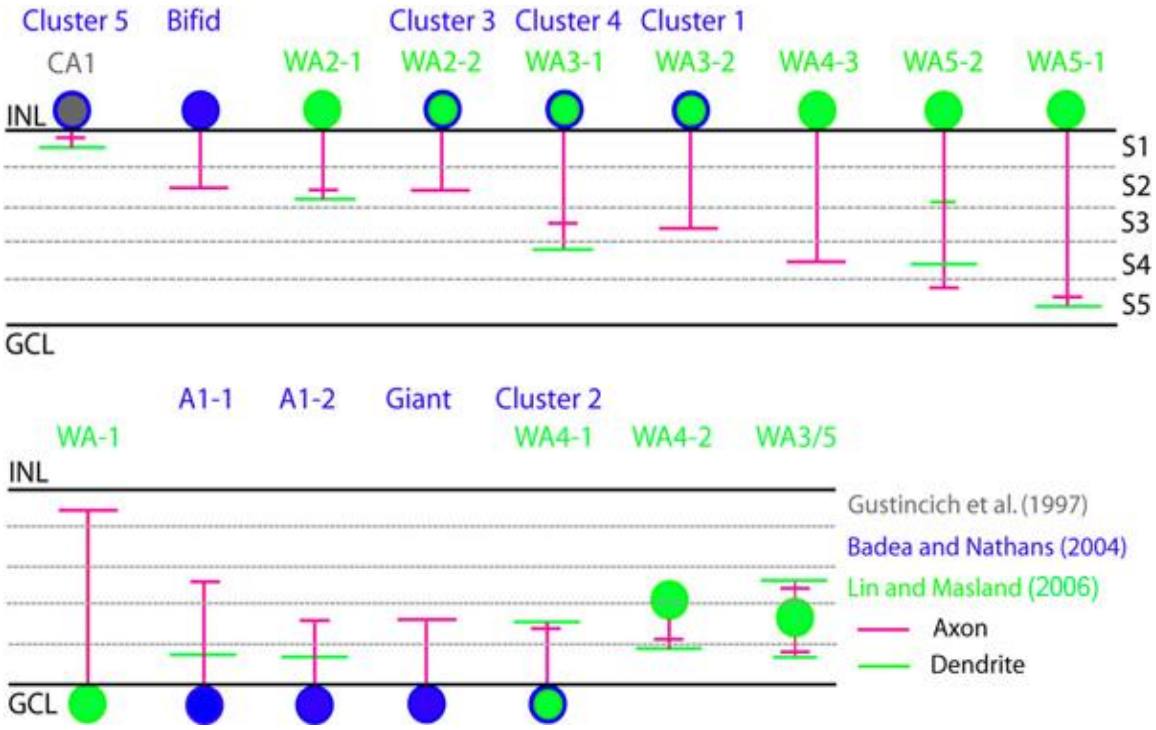

Figure 1.2. Sixteen different types of wide-field amacrine cells. (Adopted from Bin Lin and Richard H. Masland, 2006)

ii. Somatostatin-containing amacrine cells

Somatostatin (somatotropin release-inhibiting factor, SRIF) is a tetradecapeptide broadly expressed in both the peripheral and central nervous system (Epelbaum et al., 1986). SRIF was first found in ovine hypothalamic substances and characterized as an inhibitor of growth hormone release from the pituitary (Brazeau et al., 1973). SRIF is a product of a single gene with two biologically active forms: SRIF-14 and SRIF-28 (Olias et al., 2004). Although SRIF is primarily produced by cells of the PNS, CNS, and gastrointestinal tract, it is widely expressed in cells of the placenta, kidney, immune system and retina (Reichlin 1983a, 1983b; Epelbaum et al., 1994). While the somatostatinergic system is diffuse, we can study its pleiotropic functions using the mammalian retina, as both the experimental model for the central nervous system and to investigate visual processing. The functional activity of SRIF is dependent on the

activation of five distinct transmembrane G-protein-coupled SRIF subtype (sst) receptors, sst1-sst5 (Reisine et al., 1995). Due to alternative splicing, the sst2 receptor has two isoforms, sst2A and sst2B (Schindler et al., 1998; Vanetti et al., 1992). The presence of different somatostatin receptors in different retinal cell types suggests that somatostatin is synthesized and released by a subcategory of amacrine cells, but may act in a paracrine fashion to regulate neurotransmitter release (Cervia et al., 2008; Cervia and Bagnoli, 2007; Fontanesi et al., 2000). These receptors influence multiple intracellular signaling pathways, including modulation of adenylyl cyclase, guanylyl cyclase, phospholipase C and A2, tyrosine phosphatases, Nitric oxide, K+ and Ca2+ channels, Na+/H+ exchanger, and kinases (Cervia et al., 2008; Akopian et al., 2000, Petrucci et al., 2001, Raynor and Reisine, 1992). Additionally, SRIF has been implicated as a regulator of neurotransmitter release, including the release of glutamate, GABA, dopamine, and itself (Cervia et al., 2008).

iii. Dopamine-containing amacrine cells

Similar to SRIF, dopamine is a neuromodulator localized to a subset of interplexiform amacrine cells in the mammalian retina (Dowling and Ehinger, 1978). Dopamine and light have become mutually dependent partners, where dopamine's role in retinal signaling is light adaptive, and light-initiated signals can regulate dopamine production and release (Witkovsky et al., 2004; Witkovsky, 2004; Witkovsky et al., 2000). Release of dopamine can be regulated by transient and sustained light exposure, as well as a light-independent manner by glycinergic and GABAergic inhibition (Zhang et al. 2007). Dopamine works both locally at adjacent neurons and by volume transmission, where it affects the functions of a multitude of cells across the retina (Witkovsky et al., 1993). Dopamine's multiple roles in the retina are carried out by two widely distributed dopamine receptor classes, D1 and D2 (Nguyen-Legros et al., 1999) which are G-protein-coupled receptors that either increase or decrease the rate of cAMP production (Witkovsky, 2004). Additionally, DA cells express the GABA neurotransmitter and have been shown to make

GABAergic synapses on AII amacrine cells, suggesting DA cells can influence other retinal cells via slow acting metabotropic dopamine receptors and fast acting ionotropic GABA receptors (Contini et al., 2002).

iv. Novel interaction between dopamine- and somatostatin-containing amacrine cells

Previous studies have shown a correlation between SRIF and retinal dopamine release (Kouvidi et al., 2006), however, evidence of direct SRIF-containing amacrine cell modulation of dopamine-containing amacrine cells is still missing. It is postulated that SRIF's modulatory effect on dopamine (DA)-containing amacrine cells can be two-fold: GABAergic and somatostatinerigic. Furthermore, the relationship between SRIF-containing amacrine cells and DA-containing amacrine cells can be reciprocal. Kiagiadaki et al. 2007 demonstrated that the application of pharmacological dopamine receptor agonist or antagonist rather than dopamine itself can influence levels of SRIF in rat retinal explants. We suspect DA-containing amacrine cells could modulate SRIF-containing amacrine cell activity in a two-fold manner: GABAergic and dopaminergic. In this study we used immunohistochemistry, and a combination of calcium imaging and whole cell patch clamp techniques on isolated transgenic TH::RFP or TH::td-Tomato positive amacrine cells to specifically address the components and properties present in the reciprocal modulatory relationship between DA- and SRIF-containing amacrine cells.

Chapter 2. Immunohistochemical expression of tyrosine hydroxylase, somatostatin, GABA, and specific receptors in amacrine cells of mouse retina

I. Abstract

Localized to the inner retina, somatostatin and dopamine amacrine cells form an intricate morphological relationship in sublamina 1 of the IPL, and occasionally in sublamina 3 of the IPL and OPL. Somatostatin is a peptide that is widely distributed in the brain and is found in interplexiform cells and amacrine cells in the retina (Yamada et al., 1980; Smiley and Basinger, 1988; Li and Lam, 1990; Rickman et al., 1996). On the other hand, dopamine is an important circadian neuromodulator with a broad influence on cells throughout the retina. We studied the unique associations between somatostatin- and dopamine-containing amacrine cells using immunohistochemical (IHC) techniques. In wild-type and knock-in transgenic mouse lines, IHC experiments show somatostatin puncta-like processes that fasciculate along tyrosine-hydroxylase varicosities, and with thick and thin processes that stratify throughout sublamina 1 of the IPL of the retina. To determine the directionality of neuromodulation between the two amacrine cells, we used antibodies against somatostatin receptor subtype 2A (sst 2A) and D1 dopamine receptor. Results show bi-directional communication, where sst2A is found on TH-immunoreactive soma membrane and processes, and D1 colocalized with SRIF-IR soma and processes. In addition, both amacrine cell types exhibit GABAergic transmission properties. Using antibodies against GABA, VGAT, and $GABA_aR$ ($\alpha2$, $\beta2$, and $\gamma2$) subunits, we found that both amacrine cell types co-localize with each antibody in sublamina 1 of the IPL. These results suggest somatostatin- and dopamine-containing amacrine cells not only share stratification in the sublamina 1 of the IPL, but they may also have a modulatory relationship at the closely associated process. This modulatory relationship could be bi-directional, where somatostatin-containing amacrine cells could be influenced by dopamine or GABA, and dopamine-containing amacrine cells could be modulated by somatostatin or GABA.

II. Introduction

Somatostatin is a tetradecapeptide broadly expressed in both the peripheral and central nervous system, including amacrine cells of the retina (Epelbaum et al., 1986). The functional activity of SRIF is dependent on the activation of five distinct transmembrane G-protein-coupled SRIF subtype (sst) receptors, sst1-sst5 (Reisine et al., 1995). Due to alternative splicing, the sst2 receptor has two isoforms, sst2A and sst2B (Schindler et al., 1998; Vanetti et al., 1992). The presence of different somatostatin receptors in different retinal cell types suggests that somatostatin is synthesized and released by a subcategory of amacrine cells, but may act in a paracrine fashion to regulate neurotransmitter release (Cervia et al., 2008; Cervia and Bagnoli, 2007; Fontanesi et al., 2000). These receptors influence multiple intracellular signaling pathways, including modulation of adenylyl cyclase, guanylyl cyclase, phospholipase C and A2, tyrosine phosphatases, Nitric oxide, K+ and Ca2+ channels, Na+/H+ exchanger, and kinases (Cervia et al., 2008; Akopian et al., 2000, Petrucci et al., 2001, Raynor and Reisine, 1992). Additionally, SRIF has been implicated as a regulator of neurotransmitter release, including the release of glutamate, GABA, dopamine, and itself (Cervia et al., 2008).

Dopaminergic amacrine cells are a rare type of amacrine cell, amounting to less than one-hundredth of 1% of all retinal neurons (Keely and Reese, 2009). Retinal dopamine-containing amacrine neurons are rapidly activated by light, derived as an increase of tyrosine hydroxylase activity (TH). TH activity then becomes a biochemical indicator of changes in dopamine-containing cells activity; synchronized with low level in dark-adapted retinas and high in light-exposed retinas. Using antibodies against tyrosine hydroxylase, the rate limiting enzyme for dopamine production, we are able to immunohistochemically label dopamine-containing amacrine cells. Previous studies by Marshburn and Iuvone, implicate an inhibitory effect of GABA on TH activity in both dark-adapted and light exposed retinas in a biphasic manner where certain GABAergic cells activate and others show tonic inhibition (Marshburn and Iuvone, 1981). In comparison to the limited localization of TH to amacrine cells in the retina, dopamine receptors

are widely distributed throughout the retina (Veruki and Wassle, 1996), and dopamine release is thought to be synaptic, as well as extra-synaptic (Puopolo et al., 2001).

In examination of the intricate morphology seen between somatostatin- and dopamine-containing amacrine cells using immunohistochemistry, our results indicate a clear localization sst2a receptors on DA cells and D1 receptors on somatostatin cells. Besides expression of their own neuromodulators, somatostatin- and dopamine-containing amacrine cells are immuno-positive for GABA and the pre- and post-synaptic GABA neurotransmission properties.

III. Materials and Methods

i. Animals:

Retinas were collected from adult male and female C57 BL/6J mice,. The mice were maintained on a 12-hour light/dark cycle. Animal housing and all experiments were performed in accordance with the guidelines and policies for the welfare of experimental animals prescribed by the UCLA Animal Research Committee, UCLA Division of Laboratory Animal Medicine and the U.S. Public Health Service Policy on Humane Care and use of Laboratory Animals.

ii. Tissue Preparation

Mice were euthanized with an overdose of isoflurane (Novaplus, Lake Forest, IL) inhalation anesthesia and decapitated. The mouse eyes were enucleated and the cornea, iris, lens and vitreous were removed. For transverse retinal sections, eyecups were immersion-fixed in 4% paraformaldehyde (PFA) in 0.1 M phosphate buffer (PB; pH 7.4) for 15 or 30 minutes and stored overnight in 30% sucrose (in 0.1M PB) at 4°C. The eyecup was embedded in optimal cutting temperature (O.C.T.) medium (Sakura Finetek Inc., Torrance, CA) and rapidly frozen on dry ice. The eyecup was sectioned perpendicular to the vitreal surface at 12 µm thickness using a Leica 3050s Cryostat, and the sections were immediately mounted onto 2% gelatin coated slides, and stored at -20°C. For retinal whole mounts, eyecups were placed in 4%

PFA for 30 seconds. The retinas were then carefully removed and flat mounted onto clean slides, covered with a coverslip that was elevated by spacers at both ends, and fixed in 4% PFA for one hour at room temperature. Flat mounted retinas were cryoprotected with 30% sucrose solution and stored overnight at 4° C.

iii. Antibodies:

Sections and whole mounts were incubated in primary antibodies listed in Table 1 and their optimal working dilutions were determined experimentally.

Table 1. Antibodies Used in this Study

Antibody	Host	Antigen	Source	Catalog No.	Dilution
Somatostatin	Rt	Synthetic peptide corresponding to amino acids 1-14 of cyclic somatostatin conjugated to bovine thyroglobulin using carbodiimide.	Millipore Corporation, Billerica, MA	MAB354	1:100
Tyrosine Hydroxylase	Ms	Purified tyrosine hydroxylase (EC 1.14.16.2) from a rat pheochromocytoma (2)	Millipore Corporation, Billerica, MA	MAB5280	1:2000
Tyrosine Hydroxylase	Ms	Purified tyrosine hydroxylase (EC 1.14.16.2) from a rat pheochromocytoma (2)	Millipore Corporation, Billerica, MA	MAB5280X	1:2000
Tyrosine Hydroxylase	Sh	Native tyrosine hydroxylase from rat pheochromocytoma	Millipore Corporation, Billerica, MA	AB1542	1:400
Sst2A	Rb	C-terminus, Peptide: ETQRTLLNGDL-QTSI	Gramsch, Schwabhausen, Germany	SS-800	1:2000

Sst2A	RB	Synthetic peptide corresponding to the residues on the C-terminus of human Somatostatin receptor type 2	Epitomics, Burlingame, CA	3582-1	1:250
VMAT 2	Rb	Synthetic peptide consisting of the cytoplasmatic C-terminus of rat VMAT 2 (aa 496-515)	Novus Biologicals, Littleton, CO	NBP1-69750	1:1000
SNAP-25	MS	Recombinant full-length rat SNAP-25	Synaptic Systems, Gottingen, Germany	111 011	1:20,000
Syntaxin-4	Rb	Highly purified corresponding to residues 2-23 of rat or mouse Syntaxin 4	Millipore, Billerica, MA	AB5330	1:400-1:800
Syntaxin-1A	Ms	(HPC-1)	Santa Cruz	SC-12736	1:2500
DRD1	Rb	Synthesized peptide derived from human DRD1	Sigma, St. Louis, MO	SAB4500671	1:100
VGAT	Rb	Synthetic peptide AEPPVEGDIHYQR (aa 75 - 87 in rat) coupled to key-hole limpet hemocyanin via an added N- terminal cysteine	Synaptic Systems, Gottingen, Germany	131 003	1:500
GABA	Rb	GABA conjugated to BSA	Sigma, St. Louis, MO	A2052	1:1000
GABA(A) α3	Rb	Peptide corresponding to amino acids 1-15 from human GABA(A) alpha3 subunit (Swiss-Prot accession number P34903, residues 29-43 of the precursor)	Millipore, Billerica, MA	AB5594	1:2000
GABA(A) α2	Rb	Synthetic peptide (aa 29-37	Synaptic Systems,	224 103	*1:400*

		of rat GABA-A receptor α2 precursor protein) coupled to key-hole limpet hemocynanin via an added C-terminal cysteine residue.	Gottingen, Germany		
GABA(A) γ2	Rb	Synthetic peptide (aa 39-67 of mouse GABA-A receptor γ2 precursor protein) coupled to key-hole limpet hemocyanin via an added C-terminal cysteine residue.	Synaptic Systems, Gottingen, Germany	224 003	*1:400*

iv. Immunohistochemistry (IHC):

Immunostaining was carried out using the indirect immunofluorescence method on retinal sections from central and peripheral retina and whole mounts. For immunostaining of vertical cryostat sections, slides were thawed for 10 minutes on a 37°C slide warmer and then washed in 0.1 M PB for 3 times, 10 minutes each. After the final wash, retinal sections were incubated in a blocking solution of 10% normal goat serum (NGS), 1% bovine serum albumin (BSA), and 0.5% Triton X-100 in 0.1 M PB for one hour at room temperature. Sections were then incubated for 12-16 hours at 4°C in a solution consisting of 3% NGS, 1% BSA, 0.05% sodium azide, and 0.5% Triton X-100 in 0.1 M PB, pH 7.4. Sections were washed in 0.1M PB for 3 times, 10 minutes each to remove excess primary antibodies. Corresponding secondary antibodies antibodies conjugated to Alexa 568, 594 and 488 (Invitrogen, Carlsbad, CA) were diluted (1:1000) in a solution, consisting of 3% NGS, 1% BSA, 0.05% sodium azide, and 0.5% Triton X-100 in 0.1 M PB, pH 7.4. Sections were incubated in the dark for one hour at room temperature. Then, they were subsequently washed three times for 10 minutes each in 0.1M PB, air-dried and cover slipped with Aqua Poly/Mount mounting medium (Polysciences, Inc, Warrington, PA).

Retinal whole mounts were processed using a protocol similar to that used in transverse sections. Retinas were removed from sucrose solution, detached from slides and processed free-floating. First, to unmask antigen sites and improve antibody penetration, retinas were incubated in 1% sodium borohydride for one hour at room temperature. After washing in 0.1M PB for 3 times, 10 minutes each, the retinas were incubated in blocking solution for two hours at room temperature, and subsequently, placed in primary antibody solution for 3 days at 4°C. The retinas were then washed in 0.1 M PB for 3 times, 20 minutes each and incubated in the secondary antibody for 2 days at 4°C. The retinas were removed from secondary antibody solution and washed in 0.1 M PB for 3 times, 20 minutes each. Retinas were flat mounted with ganglion cell layer (GCL) up, on to unsubbed slides, air dried and cover slipped with Aqua Poly/Mount mounting medium.

For immunohistochemistry controls, all antibodies were tested using mouse retina in single immunostaining experiments to confirm specificity and optimize concentration prior to performing any double labeling experiments. Experiments omitting primary antibodies eliminated specific immunostaining. For double labeling controls, one of the two primary antibodies used for double labeling was omitted during the primary incubation step. In this case, only the immunostaining by the remaining primary antibody was detected.

v. Confocal Microscopy:

Retinal sections and whole mounts were imaged and analyzed with a Zeiss LSM 510 META laser scanning Confocal Microscopy Imager (Zeiss, Thornwood, NY). The LSM 510 is equipped with an argon (Ar) laser for 488 nm excitation, and two helium/neon (He/Ne) lasers for 543 and 633 nm excitation, respectively. Images were collected using a C-Apochromat 40x 1.2 n.a. water objective. A C-Apochromat 63x 1.2 n.a. water/oil objective was used to capture images of fibers, varicosities and contacts. Images were averaged and the scan speed and the detector gain were decreased in order to increase the signal-to-noise ratio. Images were obtained at a resolution of 2048 x 2048 pixels. The images

ranged from single scans to z-stacks of 0.5 -1 microns thick per each scan and at ~1 airy units. Z-stacks contained 5-10 optical sections with a total thickness ranging from 2.0 to 7.76 um and 2-5 sections were selected and compressed for viewing.

IV. Results

i. C57 Bl/6J retina: Expression of somatostatin

SRIF immunoreactive processes form a sparse network in the IPL adjacent to the INL and they have a dispersed network of processes into IPL laminae 3 and 5 (Bagnoli et al, 2002). Consistent with previous studies, SRIF cell bodies are in the proximal layer of the INL and the varicose fibers primarily ramify in lamina 1, 3, and 5 of the IPL, some fibers enter the INL and OPL (Figure 2.1) (Cristiani et al., 2002; Larsen et al., 1990; Sagar et al., 1985; Spira et al., 1984; Tornqvist et al., 1982; Tornqvist and Ehinger, 1988). Immunoreactive cell bodies located in the GCL are determined to be displaced SRIF amacrine cells because the lack of immunolabeling in the GC axon layer (Bagnoli et al, 2002). In order to further demonstrate this pattern of SRIF expression we used immunolabeling on whole mounts. As shown in Figure 2.1, whole mount data indicate a sparse varicose SRIF fiber stainings throughout the IPL. Furthermore, limited SRIF-IR cell bodies indicate SRIF amacrine cells have extensive lateral processes that arborize to many regions of the retina.

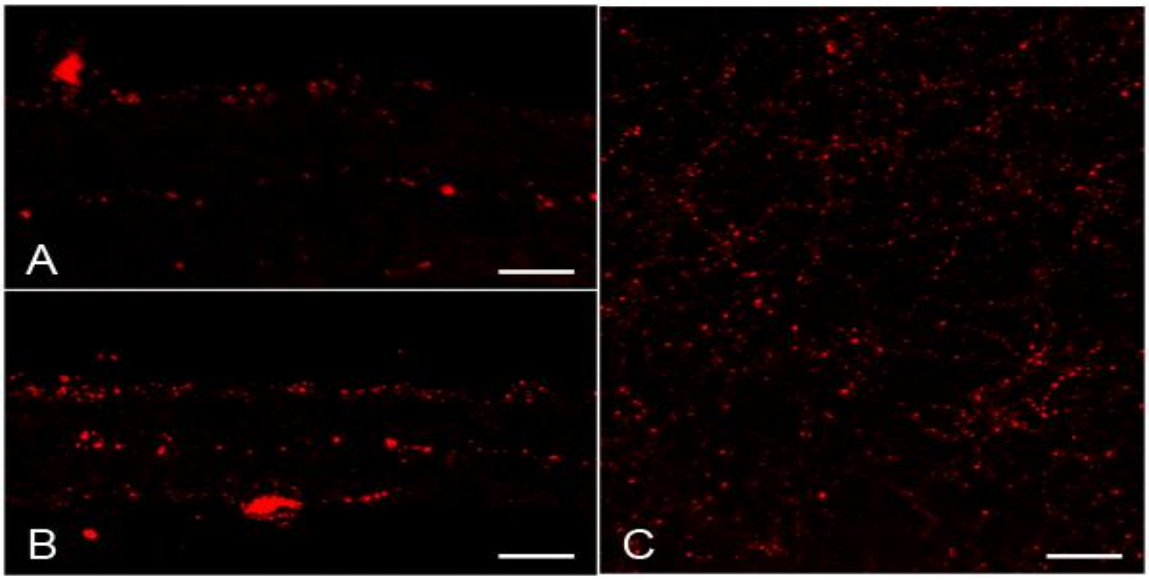

Figure 2.1. Somatostatin expression in the mouse retina. (A) SRIF-IR amacrine cell bodies lie in the INL proximal to the IPL. SRIF-IR amacrine process stratify in sublamina 1, 3, and 5 of the IPL. (B) Some SRIF-IR amacrine cell bodies are displaced into the ganglion cell layer. (C) Whole mount retina shows punctate-like SRIF-IR processes that extend across the entire retina. Scale bar = 10 µm

i. C57 Bl/6J retina: Expression of tyrosine hydroxylase

DA amacrine cells can release dopamine, as the primary neurotransmitter and neuromodulator, and GABA. To identify DA amacrine cells we used an antibody specific for TH, the rate-limiting enzyme in the synthesis of dopamine. Intensely stained TH processes primarily ramify in S1 of the OFF sublamina and a few immunostained processes were found in S3 of the IPL, and occasionally crossing into the INL to ramify in the OPL (Figure. 2.2.).

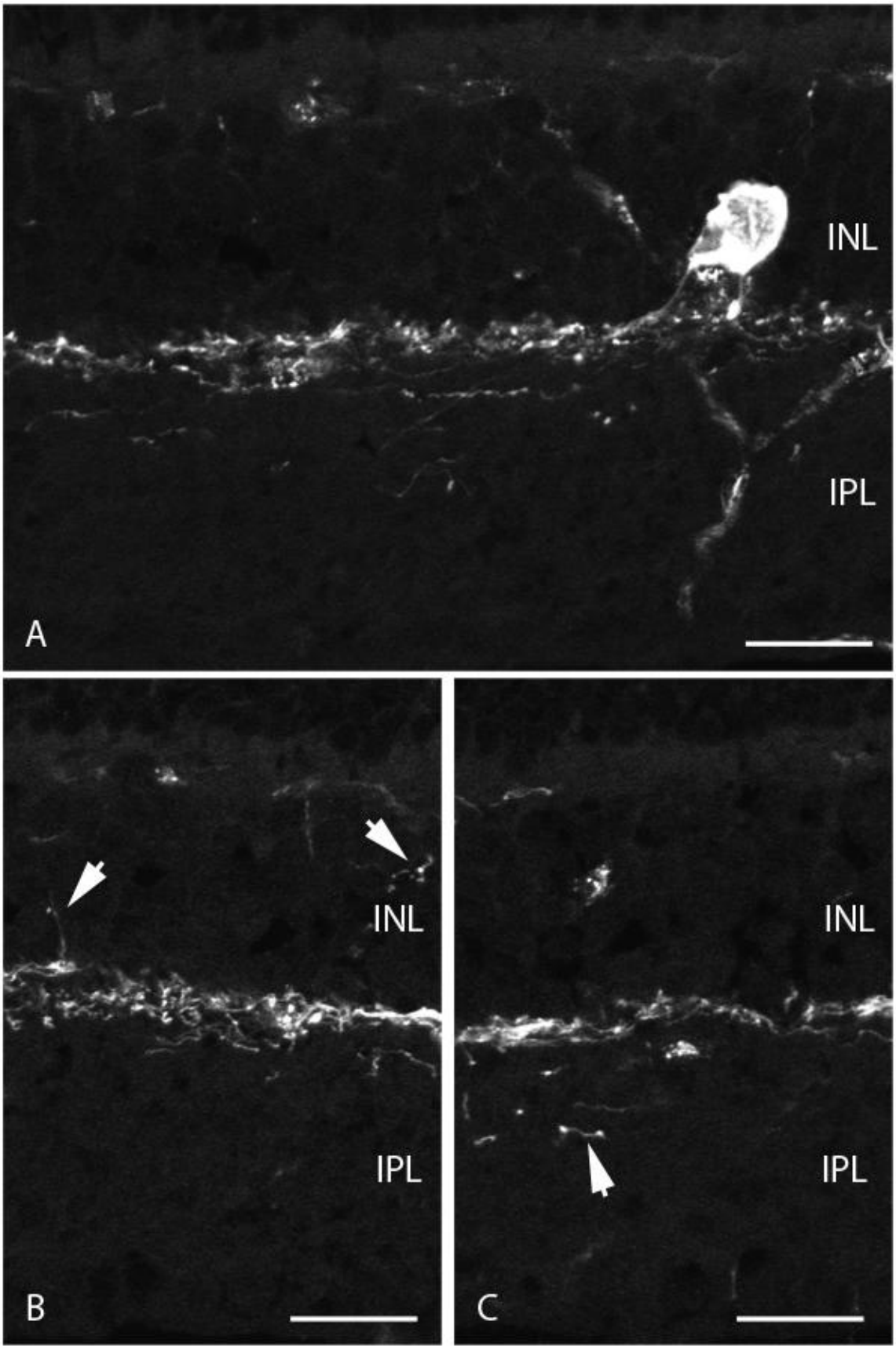
INL
IPL
A
INL
IPL
B
INL
IPL
C

Figure 2.2 Tyrosine Hydroxylase expression in mouse retina. (A) TH-IR dopamine amacrine cell bodies rest in the INL proximal to the IPL. (B) TH-IR processes mainly ramify in sublamina 1 of the IPL. Occasionally, some processes extend out through the INL, and into the OPL, as indicated by arrows. (C) Many TH-IR processes ramify in sublamina 3 of the IPL (see arrow). Scale bar = 20 µm

TH processes that ramify to the OPL usually emerge from DA axons or dendrites, rather than DA cell bodies (Witkovsky 2008). DA cell bodies are large in diameter (~20um) and reside in the INL adjacent to the IPL. Furthermore, TH-IR processes in whole mounts consisted of both fine and large diameter fibers, both of which form ring-like patterns; these rings in the TH-IR plexus are suspected to be accommodating large axons or presence of AII amacrine cells (Raviola et al., 2002, Krizaj et al. 2008). Evidence in double immunolabelings of antibodies against TH and parvalbumin (PV), a calcium binding protein, in rat retinal whole mounts suggest that DA plexus tend to surround AII amacrine cells (Contini et al., 2003).

iii.*TH and SRIF processes make contact: interaction between varicosities*

TH and SRIF immunoreactivity revealed numerous widespread contacts. Some SRIF-IR processes are adjacent to TH-IR varicosities and others are distributed throughout the arborization of fine TH-IR processes (Figure 2.3.). This suggests SRIF and TH processes are primarily in S1 and occasionally in S3 of the IPL. Double immunolabeling in both transverse and whole mount tissue revealed a unique pattern of co-stratification where TH and SRIF process run tightly together; SRIF-IR fibers tend to wrap around TH-IR cell bodies and both TH- and SRIF-IR fibers collectively encircle other amacrine cell bodies located in the INL, adjacent to the IPL. It is important to emphasize the results seen in these immunolabelings are representative of points of contact rather than co-localization; these are two distinct neuromodulators of two distinct types of amacrine cells.

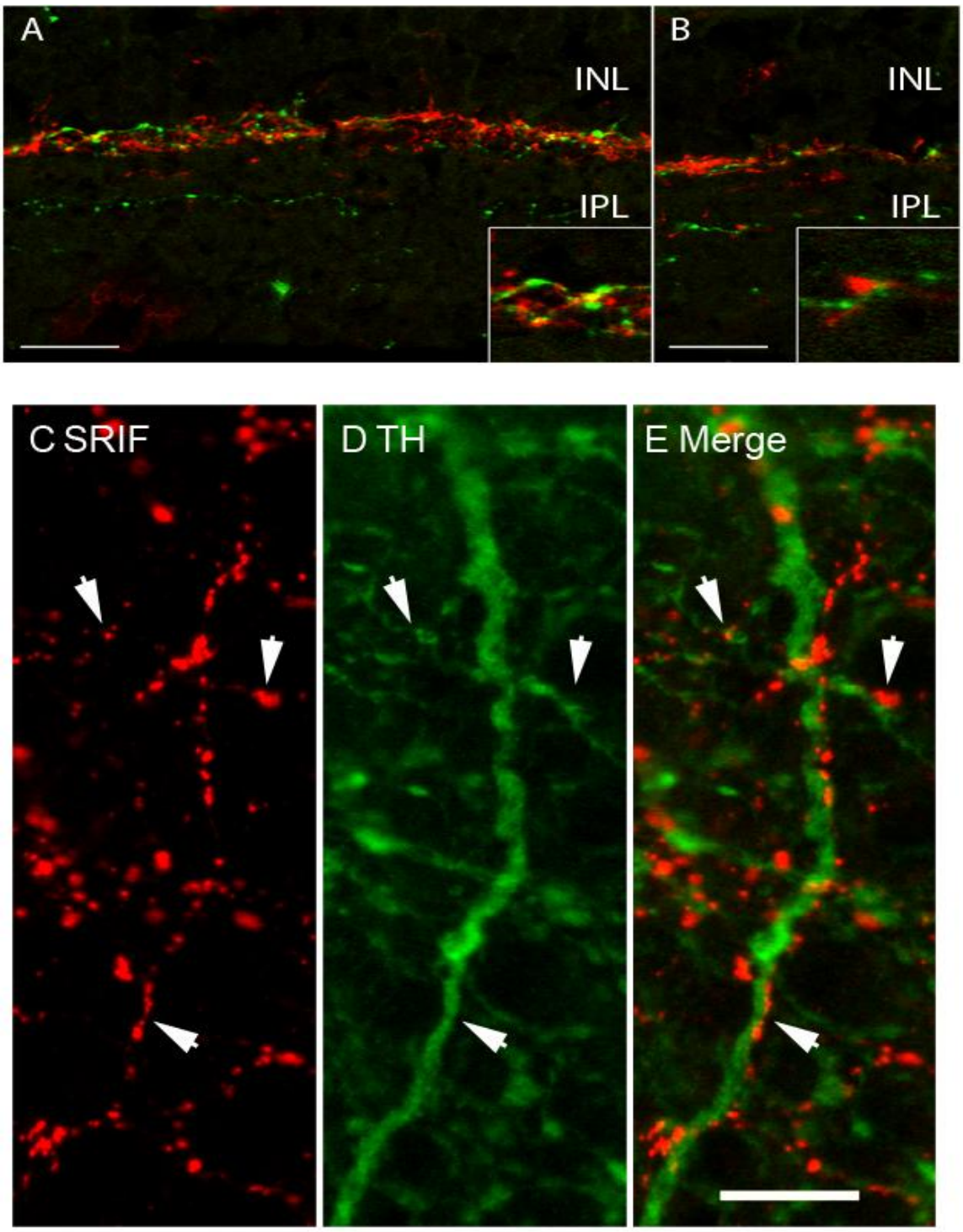

Figure 2.3. TH- and SRIF-IR processes co-fasciculate in the mouse retina. (A) TH- and SRIF-IR processes run together in sublamina 1 of the IPL. (B) TH- and SRIF-IR processes also run in close proximity in sublamina 3 of the IPL. Insets are 2X zooms, displaying the co-fasciculation of TH- and SRIF-IR varicose fibers. Scale bar = 20 µm. TH and SRIF immunolabeled whole mount retina, image taken using a 63X objective. (C) SRIF-IR fibers have a puncta-like pattern that expands the entire retina at sublamina 1 of the IPL. (D) Thick and thin TH-IR fibers are made up of many varicosities. (E) Merged

images display distinct co-fasciculation pattern between the TH- and SRIF-IR fibers (see arrows). Scale bar = 10 μm

Expression of D1 dopamine receptor, VMAT-2, and SNAP-25

SRIF-containing amacrine cells express dopamine receptor family D1

In order to assess the likely direction of neurotransmission between these contacts we employed antibodies against different dopamine receptor classes. Consistent with previous studies, D1 receptor-IR was localized to bipolar, horizontal, amacrine and ganglion cells (Veruki et al., 1996). As shown in Figure 2.4, double labeling of SRIF and D1 revealed robust co-localization in SRIF-IR cell bodies. However, due to the diffuse labeling of D1, especially along lamina 1 of the IPL, we were not able to confidently conclude complete colocalization of SRIF-IR process with D1. The significant overlap of SRIF-IR fibers with D1 labeling does suggest presence of D1 on SRIF-IR process.

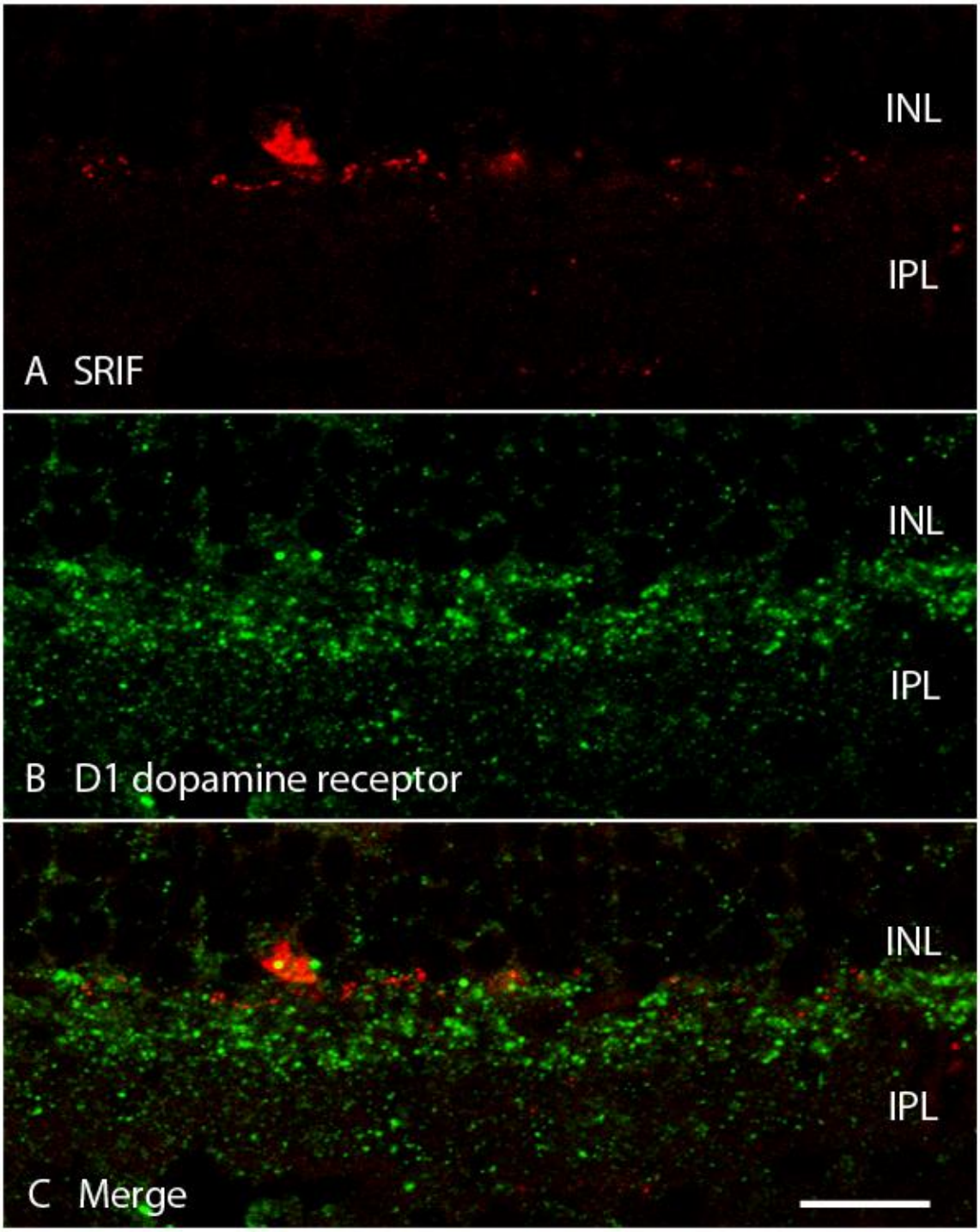

Figure 2.4. D1 dopamine receptor localization on SRIF-IR processes. (A) SRIF-IR processes extend along sublamina 1 of IPL (B) D1 dopamine receptor has no specific stratification, with diffuse labeling along sublamina 1 and 2 of the IPL. (C) Merged images indicate co-localized punctate labeling of D1 dopamine receptor and SRIF-IR varicose processes. Scale bar = 20 µm

TH colocalizes with vesicle trafficking markers: VMAT-2 and SNAP-25

To demonstrate the direction of communication at the sites of contact is from TH to SRIF, we localized vesicular markers to TH-IR processes. VMAT2 is a protein responsible for packaging dopamine into vesicles and is known to be concentrated at dopamine release sites (Hoffman et al., 1998). In the retina, VMAT2 has been localized to axonal rings of the dopaminergic plexus as well as with individual varicosities along the axons (Witkovsky et al., 2004). VMAT2-IR was punctate and widely distributed in lamina 1 of the IPL (Figure 2.5). Double immunolabelings of VMAT2 and TH revealed complete co-localization where VMAT2-IR was confined to the cytoplasm of DA cells and localized to DA cell presynaptic endings. The co-localizations were pertinent in TH fibers that extend to the OPL, lamina 1 and lamina 3 of the IPL. At TH-IR varicosities, where there is apparent contact between SRIF and TH, there are co-localized labeling of TH and VMAT2. Furthermore, in double labeling of SRIF and VMAT2, SRIF- and VMAT2-IR did not co-localize, however, there is a significant amount of contacts among the immunoreactivity, similar to the double immunolabelings between SRIF and TH-IR fibers.

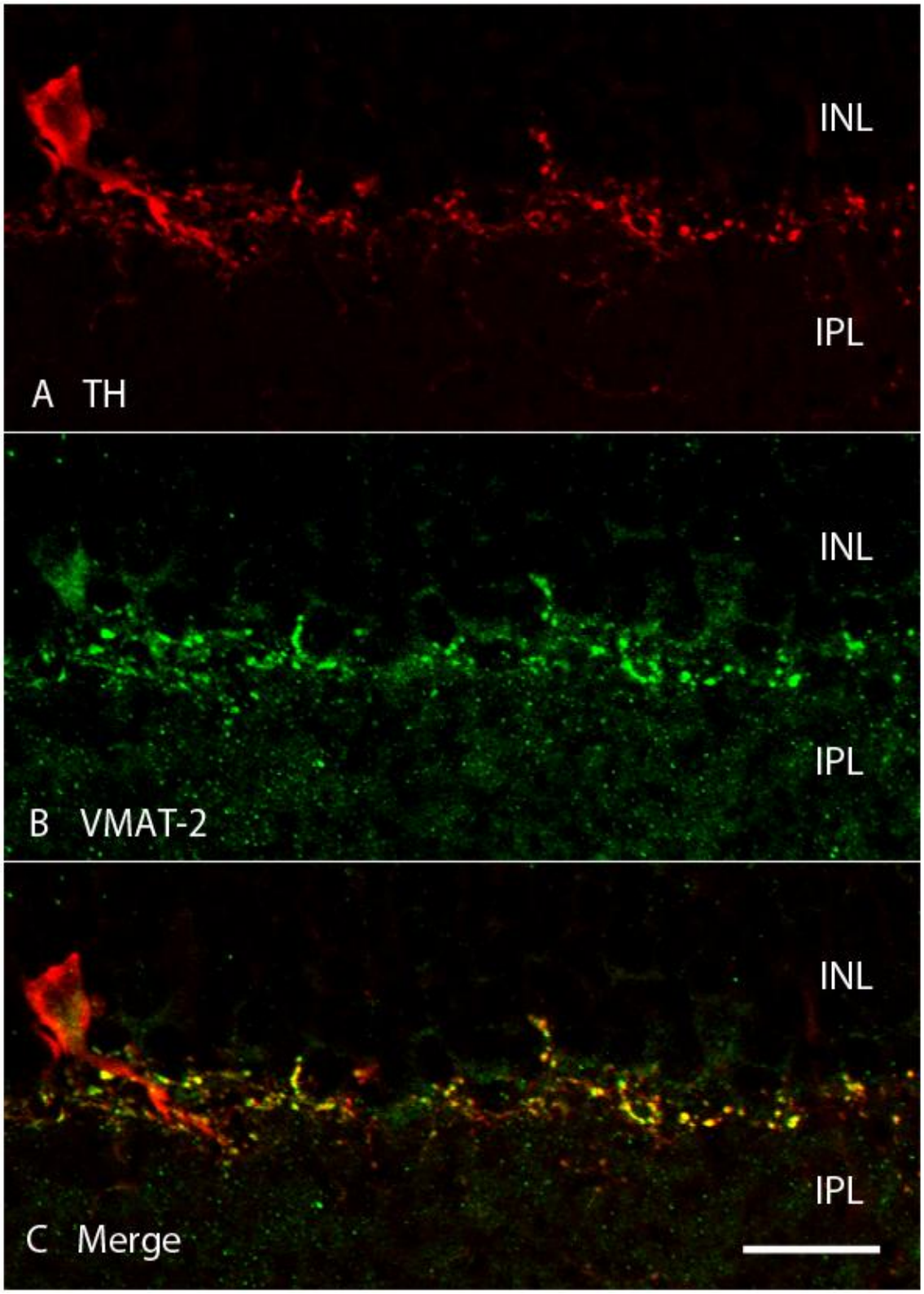

Figure 2.5. VMAT is localized to TH-IR dopamine amacrine cells. (A) TH-IR varicose processes extend along sublamina 1 and 3 of the IPL. (B) VMAT-2 labeling is punctate and mainly present in sublamina 1

of IPL. (C) Merged images show complete co-localization of VMAT-2 to TH-IR dopamine amacrine cell body in the INL, and processes in sublamina 1 and 3 of the IPL. Scale bar = 20 µm.

Besides VMAT2, TH-IR fibers were found to co-localize with another pre-synaptic vesicular trafficking protein, SNAP-25 (Figure 2.6). SNAP-25 had punctate labeling in the OPL and diffuse IR in the IPL with few punctas that arise out of the IPL into the adjacent INL. SNAP-25 was not co-labeled with SRIF-IR fibers or cell bodies (data not shown).

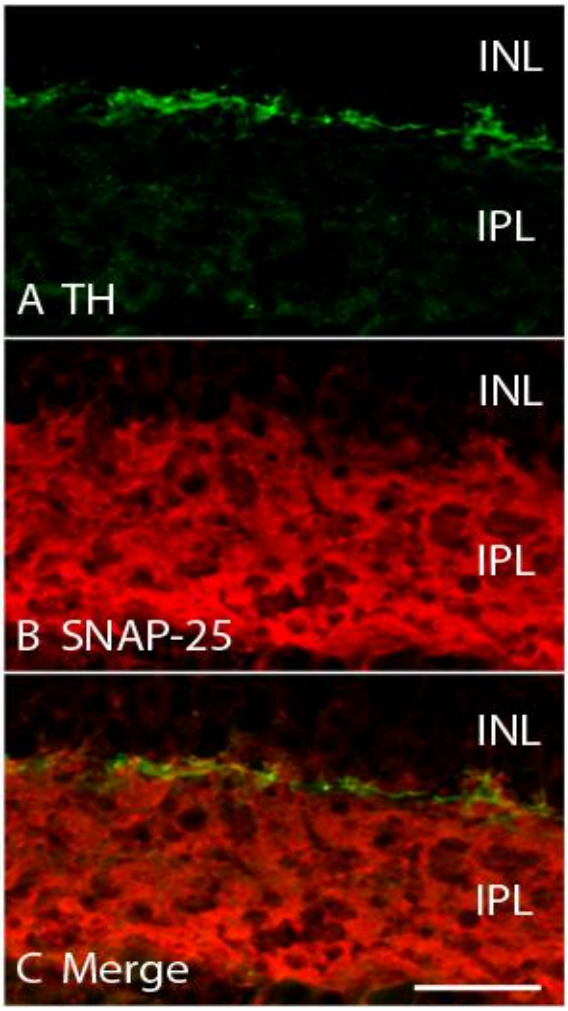

Figure 2.6. SNAP-25, a pre-synaptic marker, is localized to TH-IR dopamine process. (A) TH-IR varicose processes extend along sublamina 1 of IPL. (B) SNAP-25 labeling is diffuse and occupies every lamina of the IPL (C) Merged images show co-localization of SNAP-25 to TH-IR processes. Scale bar = 20 µm

Expression of somatostatin receptor subtype 2A (sst $_{2A}$), syntaxin-4, and syntaxin 1A

SRIF co-localizes with vesicle trafficking markers: Syntaxin 4 and Syntaxin 1A

Syntaxin-4 is a SNAP receptor protein that plays a role in mediating post-synaptic vesicular trafficking to the plasma membrane (Sherry et al., 2006). Previous studies have shown syntaxin-4 localized to horizontal cell process in the ribbon synaptic complexes of photoreceptor terminals and in puncta of the IPL and contacting dopaminergic and CD15-positive amacrine cells. Furthermore, studies show syntaxin-4 in opposition to bassoon-labeled synaptic active zones (Sherry et al., 2006). It was unclear what amacrine or interplexiform cells syntaxin-4 was localized to, but was suggested that that cell of interest was interacting with dopamine amacrine cells. To confirm the possibility of TH to SRIF communication we localized post synaptic markers on SRIF amacrine cell bodies and process. As shown in figure 2.7, syntaxin- 4 has punctate-like labeling in both the OPL and lamina 1 of the IPL. Double immunolabeling of syntaxin-4 and TH produced a similar contact staining pattern seen in TH and SRIF double immunolabelings; syntaxin-4-IR made contact with both fine and large TH-IR processes, as well as sparse labeling around the TH-IR cell bodies (data not shown). Double labeling of syntaxin-4 and SRIF revealed almost complete co-localization of syntaxin-4- and SRIF-IR fibers (Figure 2.7). In conjunction with a uni-directional TH to SRIF communication, we propose a bi-directional form of communication in which SRIF releases neurotransmitters or neuromodulators that act on TH. Staining for the pre-synaptic vesicular trafficking protein, syntaxin-1A, yielded few punctas in the OPL and wide diffuse labeling in the IPL (Figure 2.8). Double staining of syntaxin-1A and SRIF shows colocalization in SRIF-IR fibers in lamina 1 of the IPL as well as SRIF-IR cell bodies, confirming syntaxin-1 as an extrasynaptic marker that

functions in the exocytosis of neuropeptides, which can be released from any part of a neuron (Ludwig et al. 2006).

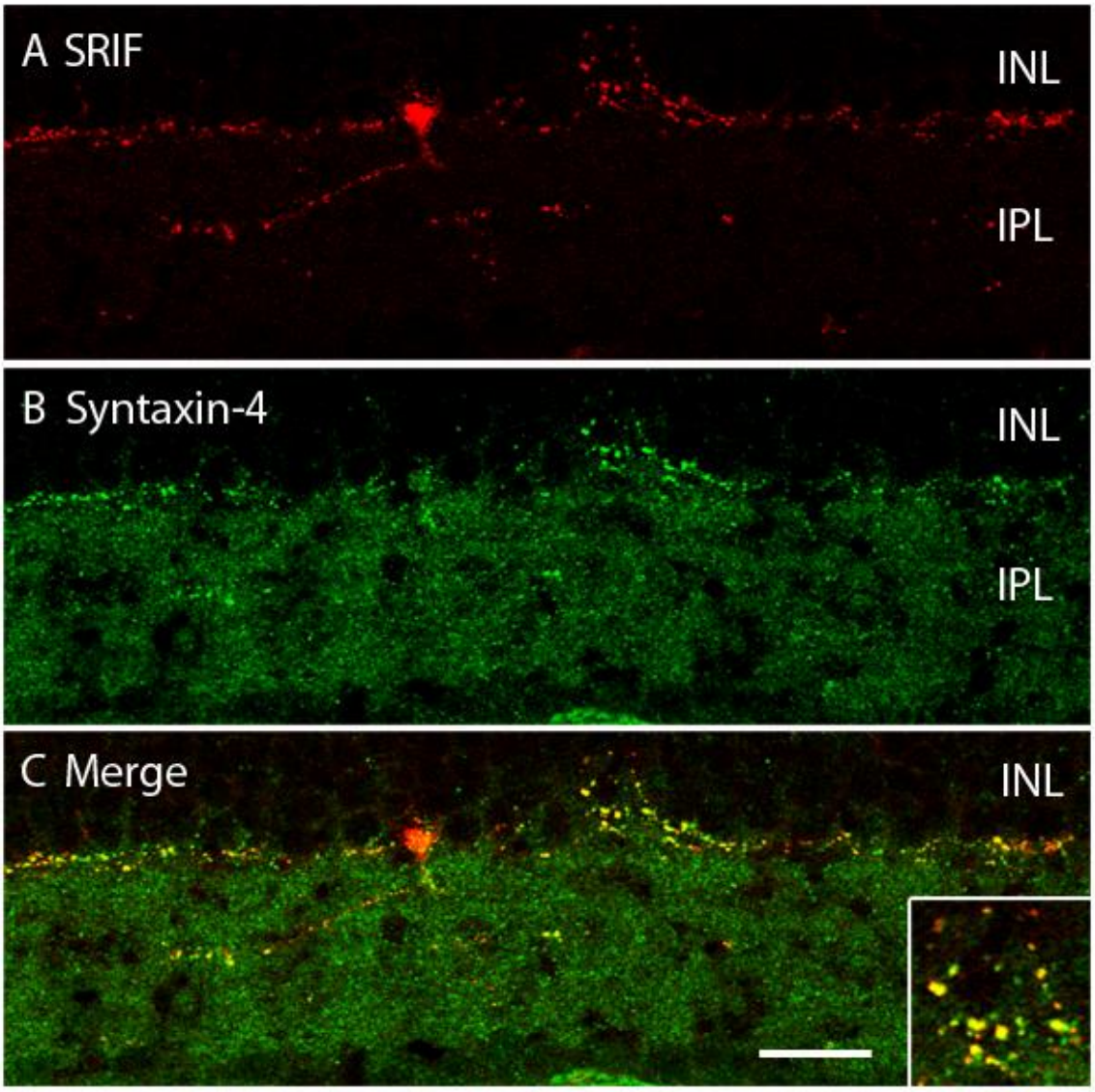

Figure 2.7. Syntaxin-4, a pre-synaptic marker, is localized to SRIF-IR amacrine process. (A) SRIF-IR puncta-like processes are present in sublamina 1, 3, and 5 of the IPL. (B) Syntaxin-4 labeling is diffuse; there are specific punctas stratifying in sublamina 1 and 3 of the IPL (C) Merged images show complete co-localization of Syntaxin-4 to SRIF-IR amacrine processes in sublamina 1 and 3 of the IPL. Inset is a 2X magnification of co-localization displayed in sublamina 1 of the IPL. Scale bar = 20 µm

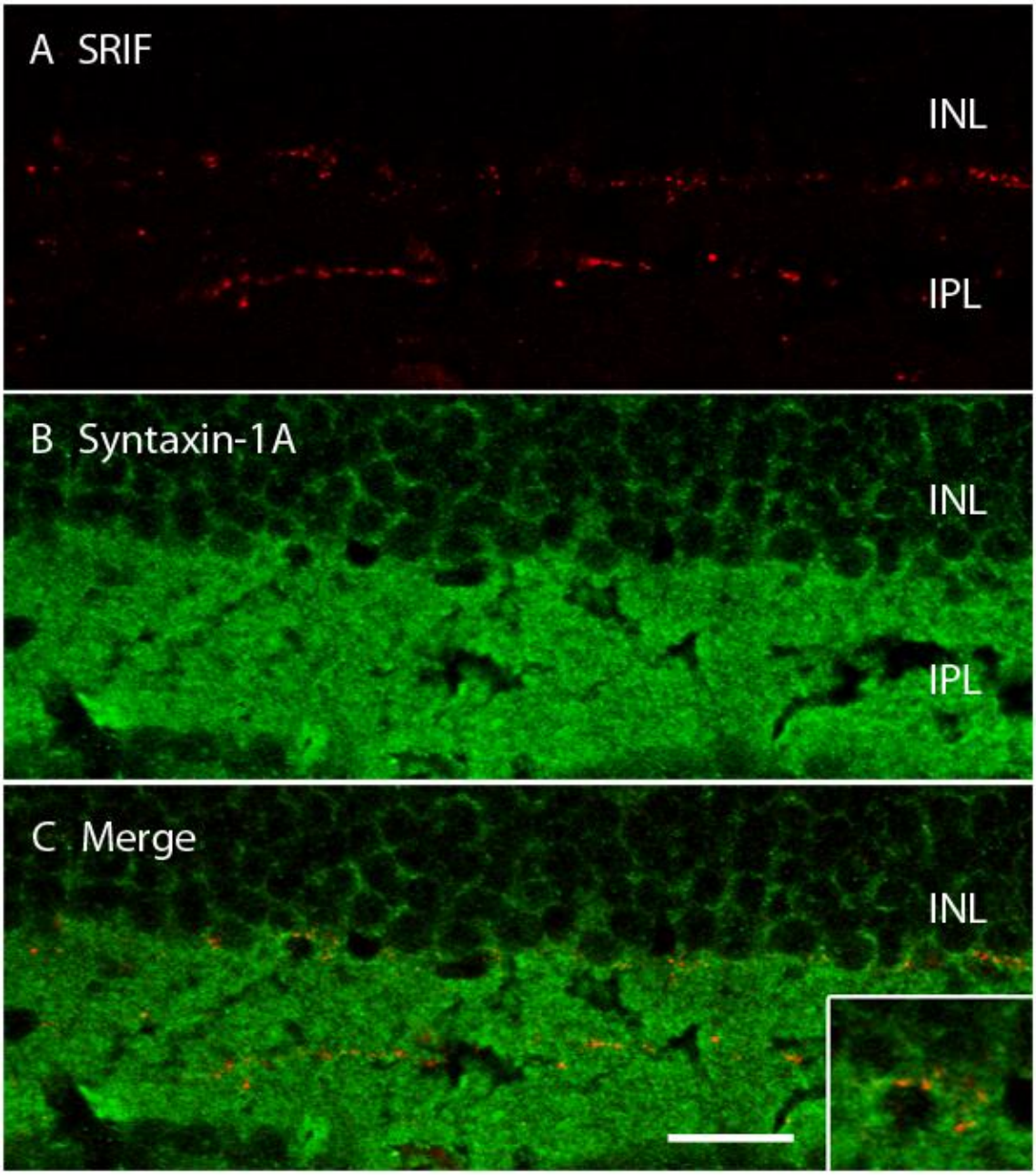

Figure 2.8. SRIF-IR amacrine process express syntaxin-1A, a pre-synaptic marker. (A) SRIF-IR varicose processes are present in sublamina 1, 3, and 5 of the IPL. (B) Syntaxin-1A labeling is diffuse and occupies every lamina of the IPL (C) Merged images show co-localization of Syntaxin-1A to SRIF-IR amacrine processes. Inset is a 2X magnification of SRIF-IR processes co-localized with syntaxin-1A. Scale bar = 20 µm

TH colocalizes with sst_{2A}

To determine the relationship of SRIF and TH varicosities, we immunolabeled transverse and whole mount retinal tissues with antibodies against sst_{2a} and TH. Sst_{2A}-IR is localized to protein kinase (PKC) immunoreactive rod bipolar cells, calbindin (CaBP) immunoreactive horizontal cells, glycinergic amacrine cells and tyrosine hydroxylase immunoreactive amacrine cells (Johnson et al., 2000). In our staining, sst_{2A} showed robust labeling of rod bipolar cells, with strongly labeled axons and axonal terminals and lightly labeled cell bodies and dendrites (Figure 2.9). Sst_{2A}-IR was also present in medium to large diameter amacrine cells located in the INL adjacent to the IPL, and their processes in lamina 1 of the IPL. Because of the intense rod bipolar cell labeling many of the amacrine cells were obscured, however, with double labeling of sst2a and TH, we see co-localization of sst_{2A} and TH immunoreactivity. Sst2a- and TH co–IR extended beyond TH-IR cell bodies and into the fine and large processes that were in close proximity and remained primarily in lamina 1 of the IPL. These results suggest SRIF can act on TH-IR cells by sst_{2A}.

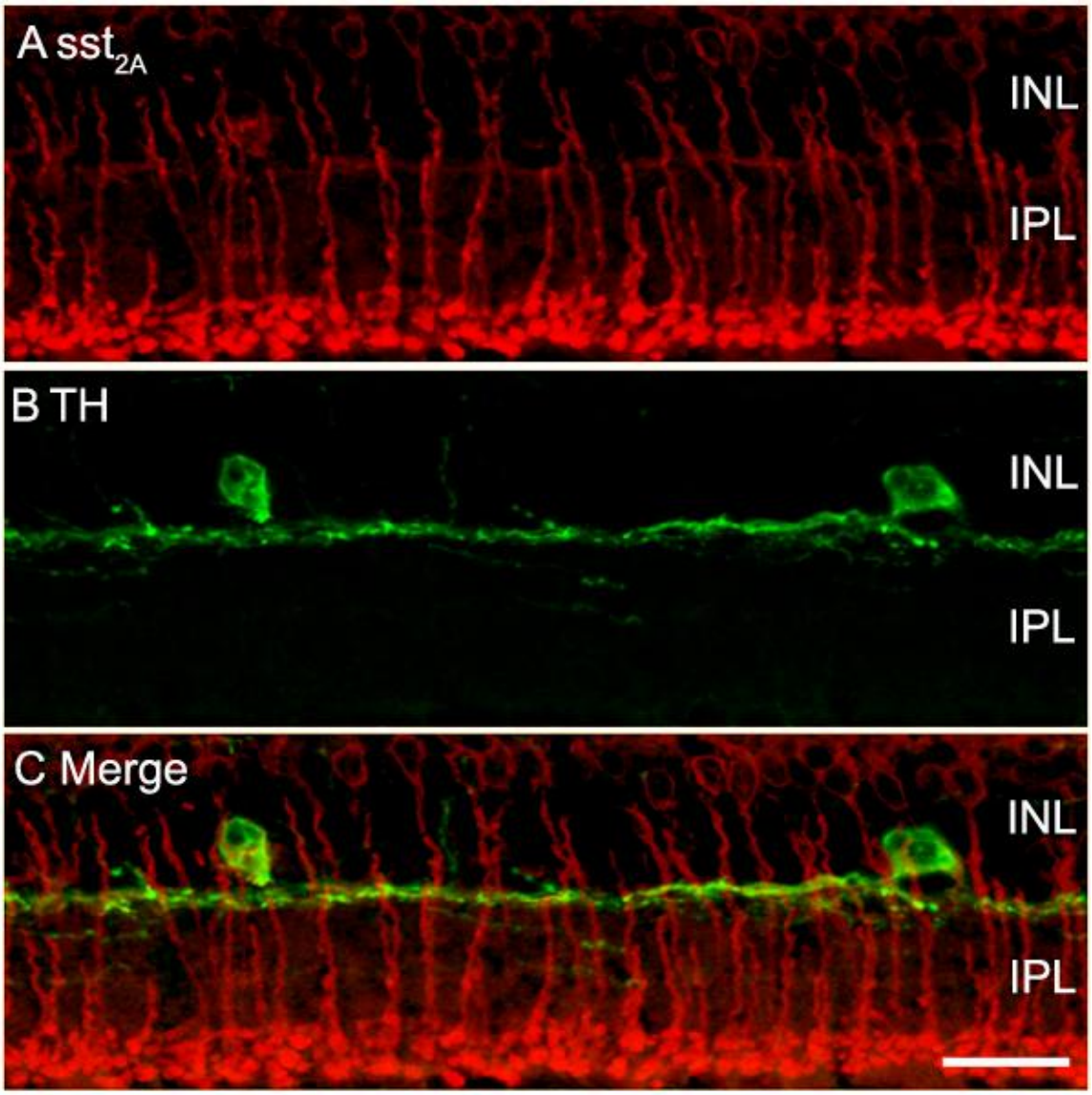

Figure 2.9. TH-IR dopamine amacrine cells express somatostatin receptor, sst_{2A}. (A) Sst_{2A} is expressed in rod bipolar cells, as well as processes along sublamina 1 of the IPL. (B) TH-IR processes are found in sublamina 1 of the IPL, and its cell bodies lie in the INL. (C) Merge images indicate co-localization of sst_{2A} receptors and TH-IR processes and cell bodies. Scale bar = 20 μm

i*v. SRIF and TH cross-talk via GABAergic synapses*

Expression of GABA and vesicular GABA transporter

Co-immunoreactivity of SRIF and TH with GABA

GABA is the main inhibitory neurotransmitter in the central nervous system and has previously been reported to be present in a subset of amacrine cells (Contini et al. 2002, Witkovsky et al. 2008, Young, 1993, Cristiani et al., 2002). Consistent with previous studies, our GABA immunolabeling was localized to amacrine cell bodies in the INL and displaced in the GCL, as well as, densely distributed in the IPL (Casini et al., 1992, Li et al., 1990, Watt et al., 1993). GABA-IR was co-localized to both TH- and SRIF-IR cell bodies in the INL, as well as, processes distributed in lamina 1 of the IPL (Figure 2.10). These double labeling studies demonstrate co-expression of TH and SRIF with GABA, and suggest neurotransmission at SRIF and TH contacts can be mediated by GABA.

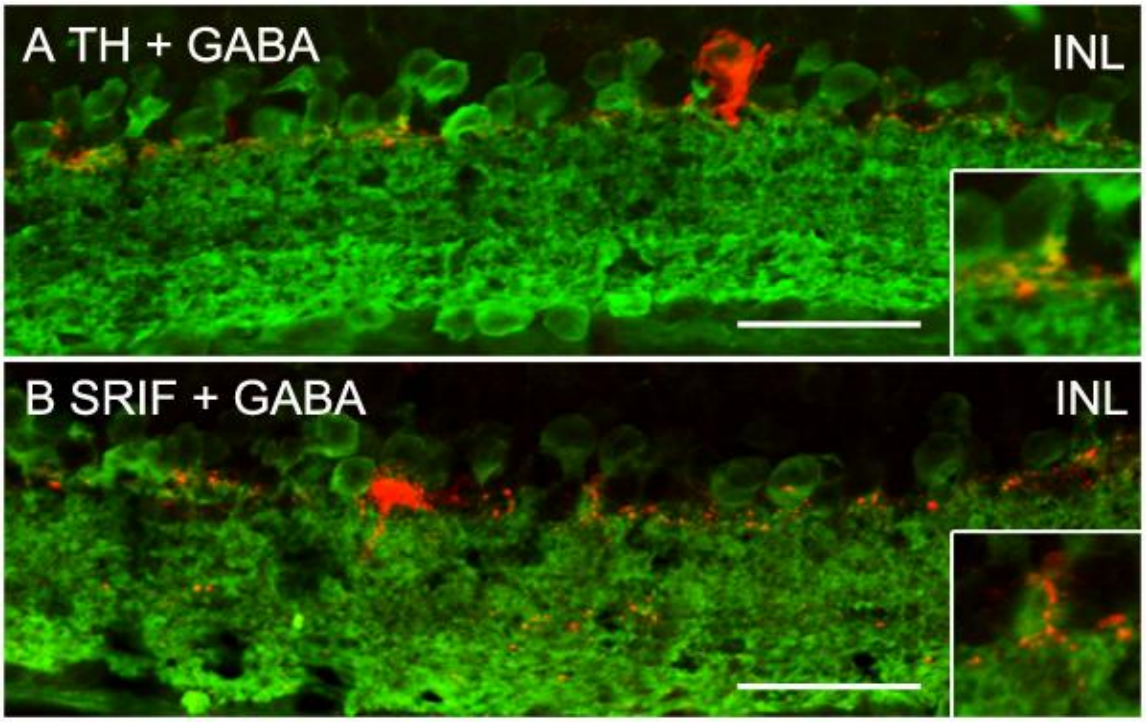

Figure 2.10. SRIF- and TH-IR processes co-localize with the inhibitory neurotransmitter, GABA (A) TH-IR cell body and varicose processes co-localize with GABA in the INL and sublamina 1 of the IPL, respectively. (B) SRIF-IR cell body and puncta-like fibers also co-localize with GABA in the INL and sublamina 1 of the IPL, respectively. Insets are a 2X magnification of the IR amacrine cell processes in sublamina 1 of the IPL that co-localized with GABA. Scale bar = 20 μm

Presence of pre-synaptic GABAergic markers

The vesicular GABA transporter (VGAT) mediates the uptake of GABA or glycine into synaptic vesicles (Chaudhry et al., 1998; McIntire et al., 1997). Investigation of VGAT expression yielded a punctate-like labeling confined to horizontal cell tips in the OPL and diffuse, but strong localization in the IPL, with faint immunostaining of horizontal cell bodies in the ONL, as well as amacrine cell bodies in the INL and displaced in the GCL (Haverkamp et al., 2000, Cueva et al., 2002, Guo et al, 2009, Guo et al., 2010, Hirano et al., 2011). Consistent with reports of VGAT being a positive indication of GABAergic neurons (Takamori et al., 2000), our double staining of VGAT with TH or VGAT with SRIF showed co-localization of VGAT-IR to TH- and SRIF-IR cell bodies and in the fine process and varicosities along lamina 1 of the IPL (Figure 2.11). These results indicate TH- and SRIF-containing amacrine cells have GABA-containing vesicles and may serve as a secondary form of neurotransmission.

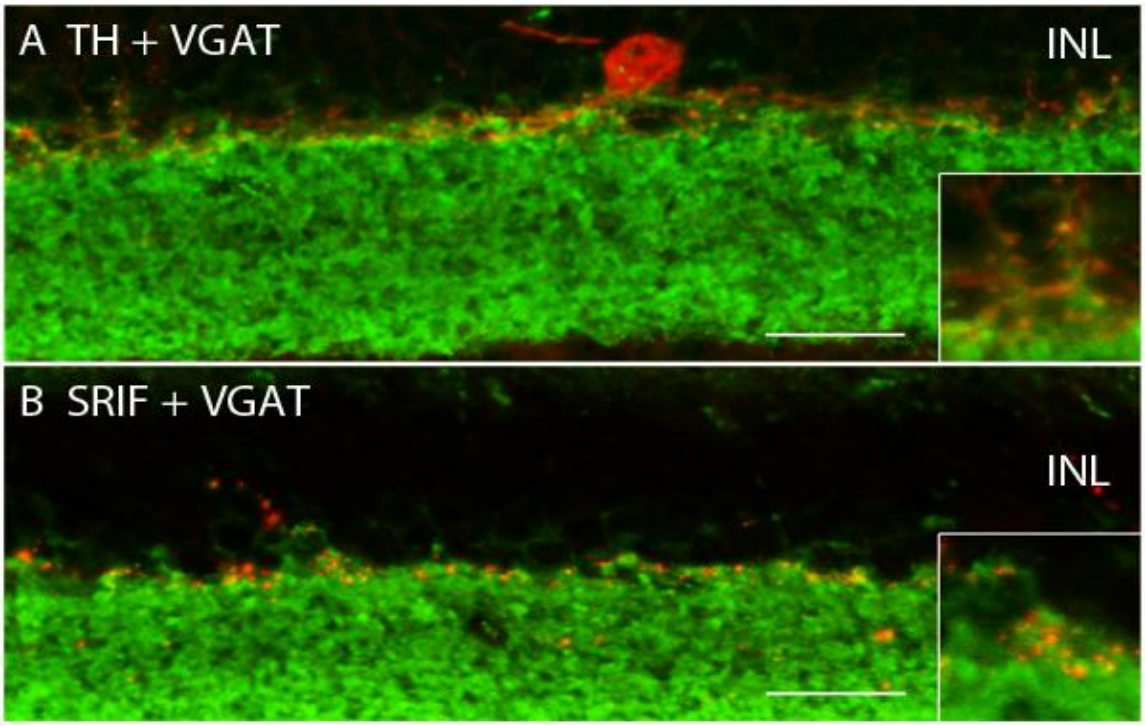

Figure 2.11. TH- and SRIF-IR amacrine cell processes co-localize with the vesicular GABA transporter, VGAT. (A) TH-IR varicose processes and soma co-localize with VGAT in the INL and sublamina 1 of the IPL, respectively. (B) SRIF-IR puncta-like fibers also co-localize with VGAT in sublamina 1 of the IPL; and the occasional process that enters the INL also expresses VGAT. Insets are a 2X magnification of the IR amacrine cell processes that co-localize with VGAT. Scale bar = 20 μm

Expression of GABA $_A$ Receptor subunits: α_2, α_3, and γ

Presence of post-synaptic GABAergic makers

GABAergic transmission is mediated by a family of receptors present on cell membrane. GABA (A) receptors make up one of three types of GABA receptor types and are well characterized ligand-gated chloride channels with fast and transient responses (Protti et al., 1997, Miller, 2008, Koulen et al., 1996. Most antibodies against the GABA (A) receptor subunits produced a punctate immunofluoresence in the IPL and were shown through electron microscopy studies as sites of GABAergic synapses (Greferath et al., 1995, Koulen et al., 1996, Wassle et al., 1998). Comparable to results shown in Greferath et al (1995), stainings with antibodies against GABA (A) α_3 produced strong punctate labeling throughout the IPL. α3 staining in the IPL was divided into three strong bands and two narrow unlabeled bands (Figure 2.12). Previous studies have shown dopaminergic amacrine cells express the GABA (A) receptor α_2, α_3, and γ_2 subunits. Consistent with double immunolabeling studies of GABA (A) α_3 with TH in rat (Greferath, et al., 1995), TH-IR cell bodies and processes in lamina 1 expressed GABA (A) α_3 (Figure 2.12). To confirm GABAergic transmission in the direction of TH- to SRIF-IR processes we investigated the co-expression of GABA (A) receptor subunits with SRIF-IR. Double immunolabeling of GABA (A) α_2, α_3, and γ_2 with SRIF produced co-localization (Figure 2.13). SRIF-IR fibers in lamina 1 and SRIF-IR cell bodies in the INL and GCL prominently expressed α_2, α_3, and γ_2 subunits. These results implicate GABA as a source of bi-directional neurotransmission between SRIF and TH-IR processes and cell bodies.

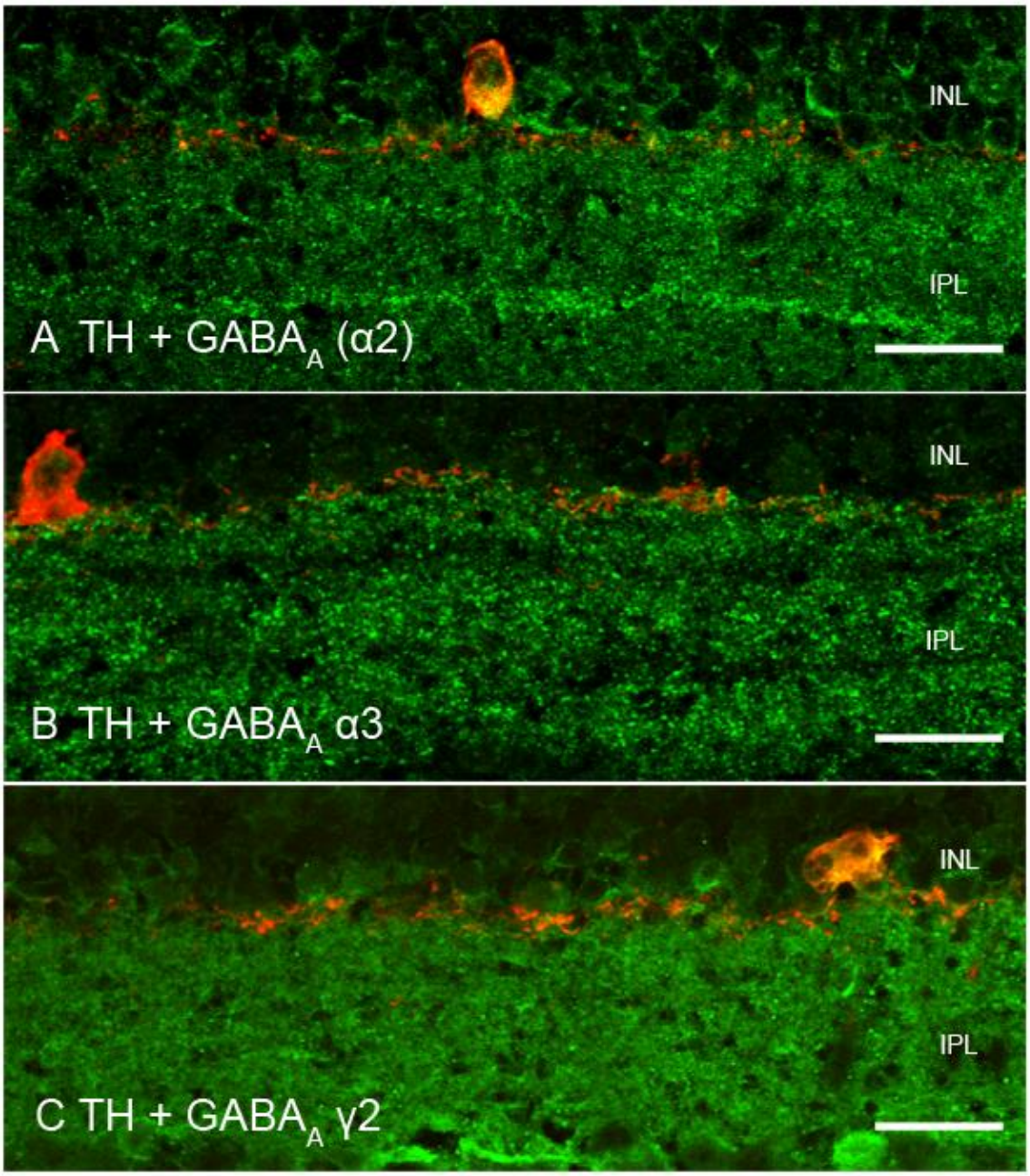

Figure 2.12. TH-IR amacrine cell somas and processes express $GABA_A$ receptor subunits. (A) TH-IR processes in sublamina 1 and displaced cell somas express $GABA_A$ α2 receptor subunits. $GABA_A$ α2 receptor subunit-IR is also found in sublamina 3 and 5 of the IPL. (B) TH-IR processes in sublamina 1 and cell somas express $GABA_A$ α3 receptor subunits. $GABA_A$ α3 receptor subunit-IR is composed of three thick bands in sublamina 1, 3, and 5 of the IPL. (C) TH-IR processes in sublamina 1 and 3, and cell soma in the INL express $GABA_A$ γ2 receptor subunits. $GABA_A$ γ2 receptor subunit-IR is diffuse throughout the IPL, with no specific lamination. Scale bar = 20 µm

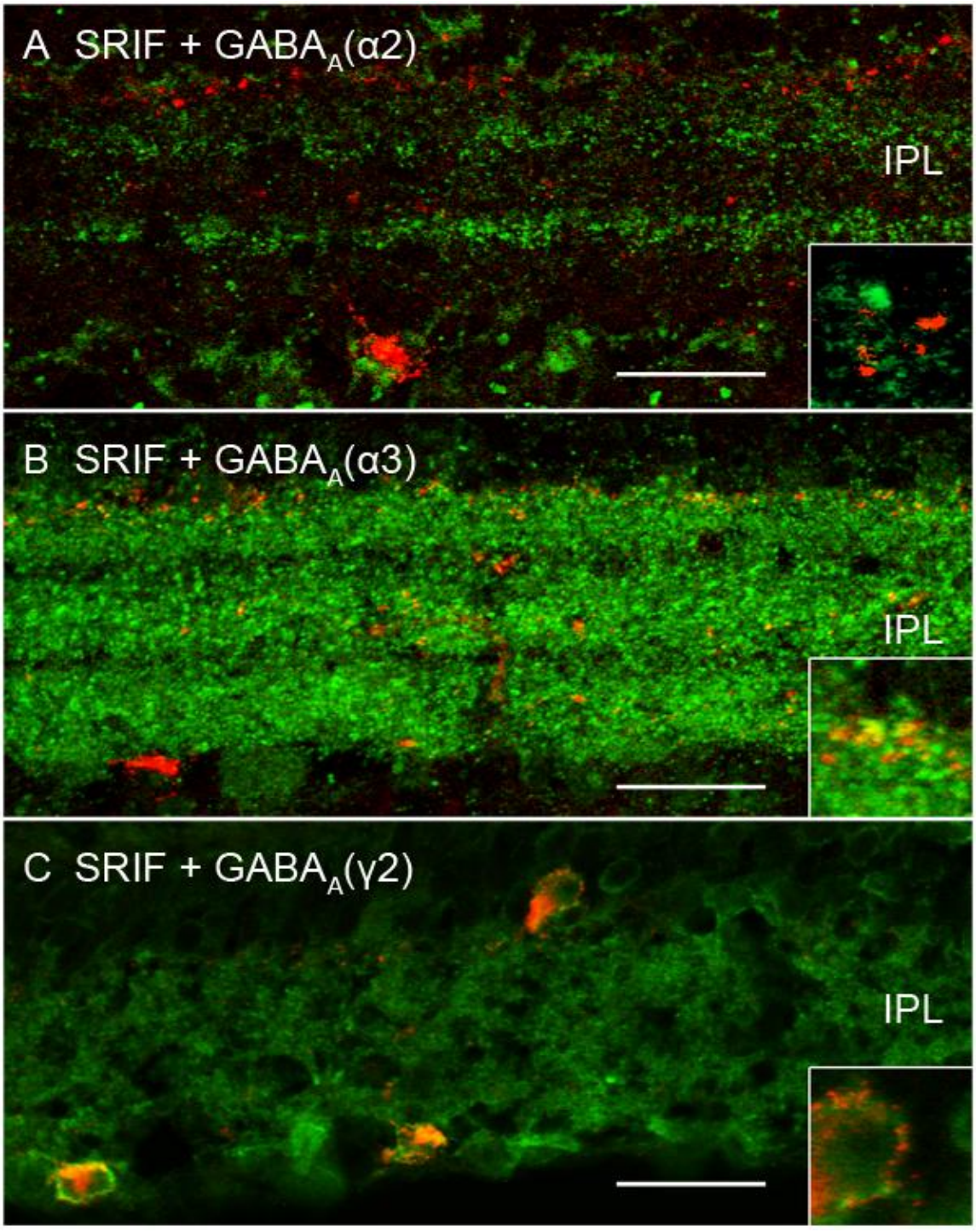

Figure 2.13. SRIF-IR amacrine cell somas and processes express $GABA_A$ receptor subunits. (A) SRIF-IR processes in sublamina 1 and displaced cell somas express $GABA_A$ α2 receptor subunits. $GABA_A$ α2 receptor subunit-IR is also found sparsely in sublamina 3 and 5 of the IPL. (B) SRIF-IR processes in sublamina 1, 3, and 5 and displaced cell soma express $GABA_A$ α3 receptor subunits. $GABA_A$ α3 receptor subunit-IR is composed of three thick bands in the IPL. (C) SRIF-IR processes in sublamina 1, 3, and 5 and cell somas in INL, as well as those displaced into the GCL express $GABA_A$ γ2 receptor subunits.

$GABA_A$ γ2 receptor subunit-IR is diffuse throughout the IPL, with no specific lamination. Insets are 3X magnification of SRIF-IR processes that co-localize with the $GABA_A$ receptor subunits in sublamina 1 of the IPL. Scale bar = 20 µm

V. Discussion

Somatostatin modulates dopamine release in the mammalian retina

Antibodies against somatostatin prominently labeled somatostatin containing amacrine cell soma and processes. Furthermore, TH immunolabeling was distributed to dopaminergic containing amacrine cell soma and large/fine processes. Detailed examination of the cellular localization of SRIF and TH immunoreactivity supports the proposed synaptic interaction between the cell types. The proposition is further supported by sst2a immuoreactivity colocalized with TH cell soma and proximal processes. These immunolabelings are also present in mouse, rat, and rabbit retinas (Johnson et al. 2000, Johnson et al. 1998, Johnson et al. 1999, Cristiani et al. 2002). Few cell bodies and vast arborization suggests SRIF can play an important global role and modulate many physiological properties of multiple retinal cell types.

Somatostatin can influence dopamine release via direct or indirect mechanisms

Somatostatin is mediated by a family of G-protein-coupled receptors; there are five molecular subtypes of SRIF receptors, sst_{1-5}. SRIF expression in the retina is widespread laterally and longitudinally, in terms of the IPL. Although it has been shown that SRIF cell body distribution throughout the mammalian retina is denser at the ventral retinal margin both in control and optic nerve transected retinas, the distribution of SRIF receptor subtypes appear to be more evenly distributed throughout all four quadrants of the retina (Cristiani et al. 2002). These findings suggest direct and indirect mechanisms of SRIF influence on the retina. Furthermore, consistent with the findings in this paper, SRIF can directly influence dopamine release via sst2a, but SRIF can also indirectly influence dopamine release by influencing rod bipolar cells and glutamate release and therefore changing the glutamatergic input to dopaminergic cell. Retinal levels

of dopamine are positively correlated with light intensity. SRIF control of dopamine implicates SRIF as a regulator of light adaptation.

Secondary form of communication between SRIF and TH amacrine cells

The close spatial proximity between retinal SRIF and TH positive processes in the mouse retina is strongly indicative of direct communication between the two systems, and is possibly bi-(or uni) directional. This conjecture has been demonstrated using both immunohistochemistry and physiological retinal slice techniques. It has been suggested that dopaminergic amacrine cells make a unidirectional monosynaptic contact with intrinsically photosensitive retinal ganglion cells (ipRGCs) (A.A. Vulger et al., 2007). However, this same conclusion has not been fully replicable in our experiments; rather we found a stronger interactive relationship between SRIF and TH. To further demonstrate our conclusion, we also attempted to delinate a secondary form of communication between the different amacrine cells. SRIF and TH could possibly communicate via the release of GABA, the predominant inhibitory neurotransmitter present in a variety of amacrine cells and horizontal cells. We report strong colocalized signals for GABA and SRIF, and GABA and TH amacrine cells. Moreover, there are several GABA receptor subtypes that also colocalize with the two amacrine cell types. GABA receptor subtypes include $GABA(A)_{\alpha 2}$, $GABA(A)_{\gamma 2}$, and $GABA(A)_{\alpha 3}$.

Chapter 3. Quantitative analysis of tyrosine hydroxylase and somatostatin immunoreactive associations

I. Abstract

Based on the immunohistochemical evidence provided in the previous chapter, dopamine- and somatostatin-containing amacrine cells form a unique morphological relationship in sublamina 1 of the IPL, and occasionally in sublamina 3 of the IPL and OPL. To the skeptic, the co-fasiculatory pattern could be a random or coincidental co-stratification of these two cells, and in actuality, these two cells may have no interactive modulatory relationship. However, using Volocity (Perkin-Elmer, Waltham, MA), we are able to quantitatively analyze the significance of contacts made between the TH- and SRIF-IR process. With whole mount retinal images stained with antibodies against TH and SRIF, we could count the number of contacts in each single z-scan. Of the two channels represented in a double-labeled whole mount retina, one color channel is held constant (non-rotated), the second color channel is either kept non-rotated (0°) or rotated in intervals of 90° (ie. 90°, 180°, 270°) and compressed for analysis in Volocity. Results from Volocity indicate that TH- and SRIF-IR fibers make contacts 41.2, 37.2, and 44.6% of the time when one of the channels were rotated 90°, 180°, 270°, respectively. Similarly TH- and VMAT-2-IR fibers made contacts 32.6, 25.8, and 23.6% of the time when one of the channels were rotated 90°, 180°, 270°, respectively. All rotated results were normalized to non-rotated contact counts. The amount of decrease in contacts made as a result of rotation is therefore the value at which contacts made in non-rotated images are significant. The quantitative analysis of morphology suggests that TH- and SRIF-IR fiber contacts are ~60% significant and may correlate with modulatory relationship between the DA- and SRIF-containing amacrine cells.

II. Introduction

Many studies within the retina have used morphology as the basis for understanding the physiological function of different cell types. Although morphology alone cannot determine functional significance,

morphology can lend some insight into potential pathways that could determine function. In order to determine whether the information given by morphological studies is a true association, there is an image rotation method that can be used to quantitatively assess the significance of co-localized activity. In particular, a recent study by Mills and colleagues looked into presence of connexin 36 (Cx36), a gap junction protein, at the AII/cone junction. Traditionally, Cx36 is known to be present at the AII/AII junction. By rotating one color channel out of phase from a double labeled immunocytochemical image, correlative associations will decrease. By comparing a non-rotated image to a rotated image, Mills and colleagues could assess whether the co-expression of Cx36 with markers of the AII/cone junction was significant, and could be controlled with images of Cx36 co-labeled with markers of AII/AII junction (Mills et al., 2001). Adopting a modified version of single color channel rotation method, here we were able to assess the significance of TH- and SRIF-IR fibers in a whole mount retinal image. Using TH- and VMAT-IR whole mount image as a control, we showed that though TH- and SRIF-IR fibers make random contacts when images are rotated, the amount of contacts is significantly decreased, suggesting the morphological pattern seen as contacts between TH- and SRIF-IR fibers is significant.

III. Materials and Methods

i. Animals:

Retinas were collected from adult male and female C57 BL/6J mice. The C57 BL/6J mice were from either Jackson Laboratory (Bar Harbor, ME) or the UCLA DLAM facility from stocks supplied by Jackson Laboratory. The mice were maintained on a 12-hour light/dark cycle. Animal housing and all experiments were performed in accordance with the guidelines and policies for the welfare of experimental animals prescribed by the UCLA Animal Research Committee, UCLA Division of Laboratory Animal Medicine and the U.S. Public Health Service Policy on Humane Care and use of Laboratory Animals.

ii. Tissue Preparation

Mice were euthanized with an overdose of isoflurane (Novaplus, Lake Forest, IL) inhalation anesthesia and decapitated. The mouse eyes were enucleated and the cornea, iris, lens and vitreous were removed. For retinal whole mounts, eyecups were placed in 4% paraformaldehyde (PFA) in 0.1 M phosphate buffer (PB; pH 7.4) for 30 seconds. The retinas were then carefully removed and flat mounted onto clean slides, covered with a coverslip that was elevated by spacers at both ends, and fixed in 4% PFA for one hour at room temperature. Flat mounted retinas were cryoprotected with 30% sucrose (in 0.1M PB) and stored overnight at 4° C.

iii. Antibodies:

Whole mounts were incubated in primary antibodies listed in Table 1 and their optimal working dilutions were determined experimentally.

Table 2. Antibodies Used in this Study

Antibody	Host	Antigen	Source	Catalog No.	Dilution
Somatostatin	Rt	Synthetic peptide corresponding to amino acids 1-14 of cyclic somatostatin conjugated to bovine thyroglobulin using carbodiimide.	Millipore Corporation, Billerica, MA	MAB354	1:100
Tyrosine Hydroxylase	Ms	Purified tyrosine hydroxylase (EC 1.14.16.2) from a rat pheochromocytoma (2)	Millipore Corporation, Billerica, MA	MAB5280	1:2000
VMAT 2	Rb	Synthetic peptide consisting of the cytoplasmatic C-terminus of rat VMAT 2 (aa 496-515)	Novus Biologicals, Littleton, CO	NBP1-69750	1:1000

iv. Immunohistochemistry (IHC):

Immunostaining was carried out using the indirect immunofluorescence method on retinal whole mounts. Retinal whole mounts were processed using a protocol similar to that used in transverse sections. Retinas were removed from sucrose solution, detached from slides and processed free-floating. First, to unmask antigen sites and improve antibody penetration, retinas were incubated in 1% sodium borohydride for one hour at room temperature. After washing in 0.1M PB for 3 times, 10 minutes each, the retinas were incubated in a blocking solution of 10% normal goat serum (NGS), 1% bovine serum albumin (BSA), and 0.5% Triton X-100 in 0.1 M PB for two hours at room temperature, and subsequently, placed in primary antibody solution of 3% NGS, 1% BSA, 0.05% sodium azide, and 0.5% Triton X-100 in 0.1 M PB, pH 7.4 for 3 days at 4°C. The retinas were then washed in 0.1 M PB for 3 times, 20 minutes each and incubated in the secondary antibody for 2 days at 4°C. The retinas were removed from secondary antibody solution and washed in 0.1 M PB for 3 times, 20 minutes each. Retinas were flat mounted with ganglion cell layer (GCL) up, on to unsubbed slides, air dried and cover slipped with Aqua Poly/Mount mounting medium (Polysciences, Inc, Warrington, PA).

For immunohistochemistry controls, all antibodies were tested using mouse retina in single immunostaining experiments to confirm specificity and optimize concentration prior to performing any double labeling experiments. Experiments omitting primary antibodies eliminated specific immunostaining. For double labeling controls, one of the two primary antibodies used for double labeling was omitted during the primary incubation step. In this case, only the immunostaining by the remaining primary antibody was detected.

v. Confocal Microscopy:

Retinal sections and whole mounts were imaged and analyzed with a Zeiss LSM 510 META laser scanning Confocal Microscopy Imager (Zeiss, Thornwood, NY). The LSM 510 is equipped with an argon (Ar) laser for 488 nm excitation, and two helium/neon (He/Ne) lasers for 543 and 633 nm excitation,

respectively. Images were collected using a C-Apochromat 40x 1.2 n.a. water objective. A C-Apochromat 63x 1.2 n.a. water/oil objective was used to capture images of fibers, varicosities and contacts. Images were averaged and the scan speed and the detector gain were decreased in order to increase the signal-to-noise ratio. Images were obtained at a resolution of 2048 x 2048 pixels. The images ranged from single scans to z-stacks of 0.5 -1 microns thick per each scan and at ~1 airy units. Z-stacks contained 5-10 optical sections with a total thickness ranging from 2.0 to 7.76 um and 2-5 sections were selected and compressed for viewing.

vi. Quantification of contact points between TH- and SRIF-IR amacrine fibers

Z-stack images (5-7 z-planes/stack, 1µm/z)from whole mount retinas double labeled with antibodies against TH and SRIF were imported into Volocity (Perkin-Elmer, Waltham, MA). Using Volocity, red and green channels were separated for each image. For rotation analysis, the red channel was rotated 90° clockwise for each z-plane. Stacks were reconstructed by reincorporating separated channels in an image sequence folder. The image sequences of each stack were deconvolved by iterative restoration using point spread functions calculated for each channel.

Following deconvolution, each z-plane was analyzed individually. SRIF and TH processes in the green and red channels, respectively, were selected by color intensity and itemized as green and red objects in Volocity. Color intensity parameters were selected to maximize recognition of processes and minimize background fluorescence. These same parameters were applied to every image stack. Also, all objects smaller than 0.75 μm^3 were excluded to reduce background interference.

Since SRIF processes typically appeared as punctate staining, they were represented by the Volocity as a series of small sized green objects that typically contacted TH processes only once. Therefore, in order to ascertain an accurate measurement of DA and SRIF amacrine processes contact points, an exclude not touching measurement item was used to count SRIF objects that contacted TH objects by selecting all

SRIF objects whose voxels either overlapped or contacted voxels of a TH object. Volocity collected raw counts and surface area data, Excel 2010 (Microsoft, Redmond, WA) was used to perform calculations, run statistical analyses and create graphical plots of the data.

IV. Results

The morphology indicates TH- and SRIF-IR fibers stratify in sublamina 1 and 3 of the IPL throughout the entire retina. More specifically, the stratification of the TH- and SRIF-IR fibers reveals a close contact relationship. Quantitative assessment of these close contacts is necessary to demonstrate significance rather than random associations. Whole mount images of TH- and SRIF- IR fibers were processed in Volocity using the single-channel rotating protocol (Figure 3.1). All values from rotated images were normalized to the non-rotated image. Post-Volocity analysis shows that there is a 58.8, 62.8, and 55.4% decrease in TH- and SRIF-IR fiber contacts when one of the channels are rotated 90°, 180°, and 270°, respectively. This suggests that the 41.2, 37.2, and 44.6% that are still making contacts after 90°, 180°, and 270°, respectively, are contacts that are made by chance (Figure 3.2). As a control, analysis of TH-IR and VMAT-2 –IR (completely co-localized in non-rotated images), yielded a 67.4%, 74.2%, and 76.4% decrease in contacts when one of the channels are rotated 90°, 180°, and 270°, respectively. Again, the 32.6, 25.8, and 23.6% that continue to make contacts in 90°, 180°, and 270° rotated images, respectively, are considered non-specific or 'random' associations that are made by chance, and not indicative of true contacts (Figure 3.3). The average percentage of random-associations seen in the TH- and SRIF-IR contact counts is comparable to the percentage seen in TH- and VMAT-2-IR contact counts, where TH- and SRIF-IR counts was slightly higher. In the 90°, 180°, and 270° rotated images, TH- and VMAT-IR fibers make contacts on average 27% (x) of the time, whereas TH- and SRIF-IR fibers make contacts 41% (y) of the time. As shown in figure 2.5, TH and VMAT-2 are co-localized; therefore any contacts that were made in the rotated images would be deemed random and made by chance. The greater amount

of contacts (y - x = 14%) in the rotated TH- and SRIF-IR contact counts could be a result of background fluorescence, random-associations, or real associations.

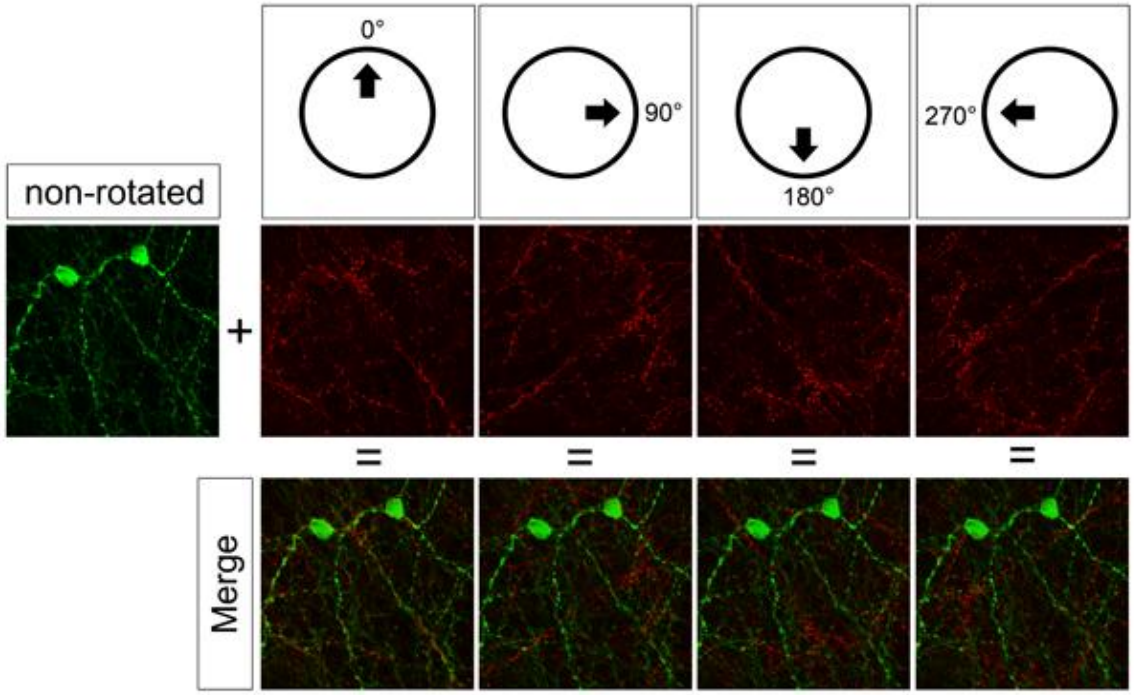

Figure 3.1. TH- and SRIF-IR whole mount retina contact count analysis. Using Volocity, a single channel from a double labeled image is rotated in 90° intervals, starting with a non-rotated image. Merged images of non-rotated channel and channel rotated in 0°, 90°, 180°, or 270° are used for analysis in Volocity. Contacts are counted from a single z-scan, 1 µm per each z-scan.

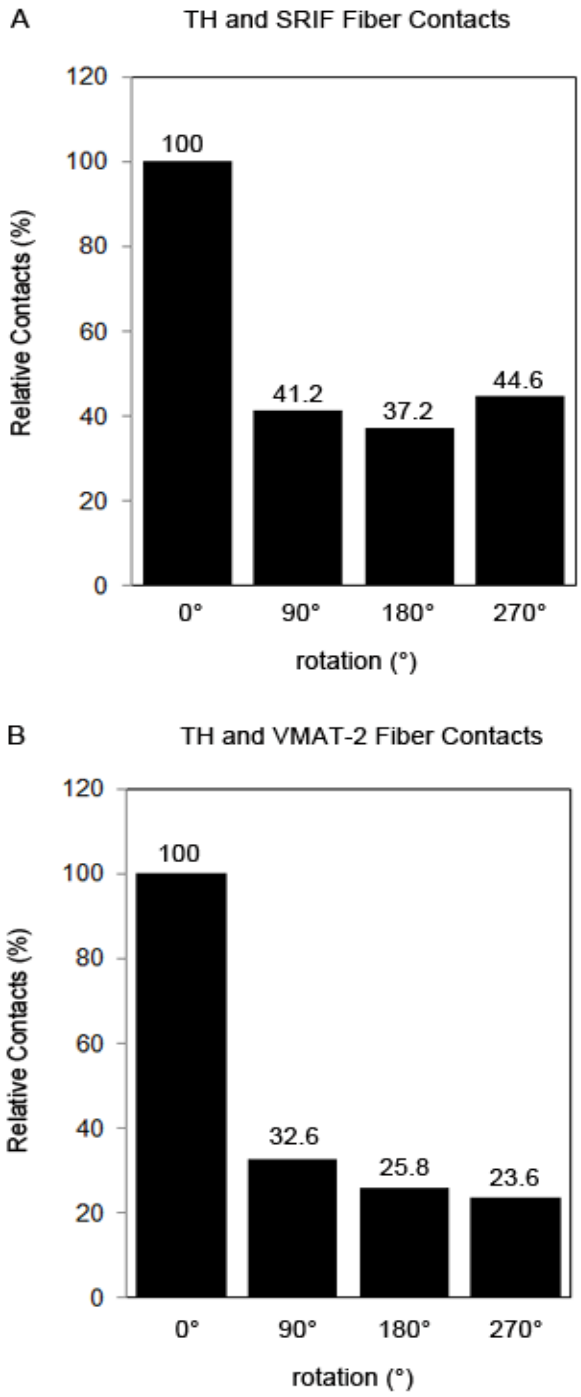

Figure 3.2. TH and SRIF fiber contact quantitative analysis. (A) Rotation of one of the channels by 90°, 180°, and 270° renders a 58.8%, 62.8%, and 55.4% decrease, respectively, in number of contacts between

the fibers in a TH and SRIF immunolabeled wholemount retina image. (n = 28 scans; 5 animals) (B) Rotation of one of the channels by 90°, 180°, and 270° renders a 67.4%, 74.2%, and 76.4% decrease, respectively, in number of contacts between the fibers in a TH and VMAT-2 immunolabeled wholemount retina image. (n = 29 scans; 4 animals) Count analysis were done using Volocity and Excel.

V. Discussion

Although morphology offers many clues about possible physiological functions, there is a limited amount of confidence that we can put in morphology to tell us the complete story about a cell's function and or secondary influences (paracrine action). However, we cannot disregard the information that morphology can suggest about a system's functional properties. Recent studies looking at the localization of gap-junction proteins, connexin 36, 45, and 57, in different retinal cell types, used morphological assays such as dye injection and immunocytochemistry. In order to assess significance seen in the co-localized labeling, a one-color channel rotation was used to determine true colocalization versus false positive colocalization (Mills et al., 2001; Hilgen et al., 2011; Pan et al., 2012). Using the one-color channel rotation method we can quantitatively assess the significance of the morphological pattern. However, because the one color channel rotation method is more commonly used to address significance of co-localized labeling of double labeled images we adopted a modified one color channel rotation paradigm to count and assess the level of association between different cells that are not co-localized but appear to have a close contact relationship. Our results indicate that though the method was designed for co-localized assessments, the values of true contacts versus false positive contacts, found in the TH- and SRIF-IR, were similar when compared to the control of true colocalization versus false positive colocalization, found in the TH- and VMAT-2-IR. Therefore, we are able to quantitatively understand the significance of the associated processes, and confirm morphological significance. Ultimately to fully understand a cells functional modulation it is necessary to carry out functional assays.

Chapter 4. Physiological evidence of reciprocal modulation between dopamine- and somatostatin-containing amacrine cells using TH::RFP and TH::td-tomato transgenic mouse lines

I. Abstract

Somatostatin (SRIF) is known to modulate the levels of dopamine-containing amacrine cells, but the membrane mechanism and the degree of intracellular calcium signaling by which SRIF modulates the DA amacrines remains unclear. Using two transgenic mouse models we address SRIF's modulation of DA amacrine cells. Immunohistochemical studies were performed to confirm that the two mouse models express the proper cells, and whether morphological pattern seen in C57 BL/6J between TH- and SRIF-IR fibers is also present. Calcium imaging studies were used to assess the effects of SRIF peptide (100 μM - 100 nM) and L-054,264 (1-10 μM) (sst_{2A} agonist) stimulation on intracellular calcium levels in DA amacrine cells. Changes in intracellular calcium in response to a depolarization induced by elevated [K^+] were recorded using Fluo-4, calcium indicator dye. In preliminary electrophysiological assays on isolated amacrine cells, we show that somatostatin peptide increased the outward K^+ current by 16.7% in whole cell patch-clamped DA amacrine cells. The suppression of spiking and Ca2+ signaling by SRIF peptide and L-054,264 suggests that SRIF has an inhibitory modulation of DA amacrine cells neurotransmission by acting on the sst_{2A} receptor.

II. Introduction

In the mammalian retina, somatostatin, expressed by a subset of amacrine cells, can modulate several different retinal cell types by acting on its broadly expressed receptors. In a study by Farrell et al., isolated rat retinal ganglion cells showed reduced spiking and increased outward K+ by 51.1% in the presence of L-803,087, a selective sst_4 agonist. In photoreceptor terminals, somatostatin elicits an increase in a delayed rectifier K^+ current (I_{KV}), a decrease in L-type Ca^{2+} (I_{Ca}) current in rods, and an increase in I_{Ca} in cones (Akopian et al., 2001). In rabbit bipolar cells, somatostatin inhibits calcium-activated K^+ (BK) channel through the inhibition of L-type Ca^{2+} channels (Petrucci et al., 2001). In a separate experiment on

rat rod bipolar cells, somatostatin inhibits high K^+ evoked increases of intracellular Ca^{2+} concentration ($[Ca^{2+}]_i$) (Johnson et al., 2001). Alternatively, somatostatin, BIM23014 (sst_2 agonist), and L797.591 (sst_1 agonist) was shown to increase dopamine levels in a concentration-dependent manner, whereas CYN154806 (sst_2 antagonist) reversed the actions of somatostatin (Kouvidi et al., 2005).

The objective of this study is to address the effects of somatostatin and the sst_{2A} agonist on isolated DA amacrine cells in terms of the membrane excitability and intracellular calcium signaling.

III. Materials and Methods

i. Animals:

Retinas were collected from adult male and female transgenic mouse models. The first transgenic mouse model expresses red fluorescent protein (RFP) under the control of the TH promoter (Zhang et al., 2004). The second transgenic mouse model express td-tomato under the control of a TH-CRE promoter. The TH::RFP transgenic line (Zhang et al., 2004) was a generous donation from Dr. Douglas G. McMahon of Vanderbilt University. The TH::td-tomato transgenic line was developed in the UCLA Division of Laboratory Animal Medicine breeding colony from TH-CRE and td-tomato (ROSA-26) mice supplied by Jackson Laboratory (Bar Harbor, ME). The mice were maintained on a 12-hour light/dark cycle. Animal housing and all experiments were performed in accordance with the guidelines and policies for the welfare of experimental animals prescribed by the UCLA Animal Research Committee, UCLA Division of Laboratory Animal Medicine and the U.S. Public Health Service Policy on Humane Care and use of Laboratory Animals.

ii. Tissue Preparation

Mice were euthanized with isoflurane (Novaplus, Lake Forest, IL) inhalation anesthesia and decapitated. The mouse eyes were enucleated and the cornea, iris, lens and vitreous were removed. For retinal whole mounts, eyecups were placed in 4% paraformaldehyde (PFA) in 0.1 M phosphate buffer (PB; pH 7.4) for

30 seconds. The retinas were then carefully removed and flat mounted onto clean slides, covered with a coverslip that was elevated by spacers at both ends, and fixed in 4% PFA for one hour at room temperature. Flat mounted retinas were cryoprotected with 30% sucrose (in 0.1M PB) and stored overnight at 4° C.

iii. Antibodies:

Whole mounts were incubated in primary antibodies listed in Table 1 and their optimal working dilutions were determined experimentally.

Table 3. Antibodies Used in this Study

Antibody	Host	Antigen	Source	Catalog No.	Dilution
Somatostatin	Rt	Synthetic peptide corresponding to amino acids 1-14 of cyclic somatostatin conjugated to bovine thyroglobulin using carbodiimide.	Millipore Corporation, Billerica, MA	MAB354	1:100
Tyrosine Hydroxylase	Ms	Purified tyrosine hydroxylase (EC 1.14.16.2) from a rat pheochromocytoma (2)	Millipore Corporation, Billerica, MA	MAB5280	1:2000

iv. Immunohistochemistry (IHC):

Immunostaining was carried out using the indirect immunofluorescence method on retinal whole mounts. Retinal whole mounts were processed using a protocol similar to that used in transverse sections. Retinas were removed from sucrose solution, detached from slides and processed free-floating. First, to unmask antigen sites and improve antibody penetration, retinas were incubated in 1% sodium borohydride for one

hour at room temperature. After washing in 0.1M PB for 3 times, 10 minutes each, the retinas were incubated in a blocking solution of 10% normal goat serum (NGS), 1% bovine serum albumin (BSA), and 0.5% Triton X-100 in 0.1 M PB for two hours at room temperature, and subsequently, placed in primary antibody solution of 3% NGS, 1% BSA, 0.05% sodium azide, and 0.5% Triton X-100 in 0.1 M PB, pH 7.4 for 3 days at 4°C. The retinas were then washed in 0.1 M PB for 3 times, 20 minutes each and incubated in the secondary antibody for 2 days at 4°C. The retinas were removed from secondary antibody solution and washed in 0.1 M PB for 3 times, 20 minutes each. Retinas were flat mounted with ganglion cell layer (GCL) up, on to unsubbed slides, air dried and cover slipped with Aqua Poly/Mount mounting medium (Polysciences, Inc, Warrington, PA).

For immunohistochemistry controls, all antibodies were tested using mouse retina in single immunostaining experiments to confirm specificity and optimize concentration prior to performing any double labeling experiments. Experiments omitting primary antibodies eliminated specific immunostaining. For double labeling controls, one of the two primary antibodies used for double labeling was omitted during the primary incubation step. In this case, only the immunostaining by the remaining primary antibody was detected.

v. Confocal Microscopy:

Retinal sections and whole mounts were imaged and analyzed with a Zeiss LSM 510 META laser scanning Confocal Microscopy Imager (Zeiss, Thornwood, NY). The LSM 510 is equipped with an argon (Ar) laser for 488 nm excitation, and two helium/neon (He/Ne) lasers for 543 and 633 nm excitation, respectively. Images were collected using a C-Apochromat 40x 1.2 n.a. water objective. A C-Apochromat 63x 1.2 n.a. water/oil objective was used to capture images of fibers, varicosities and contacts. Images were averaged and the scan speed and the detector gain were decreased in order to increase the signal-to-noise ratio. Images were obtained at a resolution of 2048 x 2048 pixels. The images ranged from single scans to z-stacks of 0.5 -1 microns thick per each scan and at ~1 airy units. Z-stacks

contained 5-10 optical sections with a total thickness ranging from 2.0 to 7.76 um and 2-5 sections were selected and compressed for viewing.

vi. *Acute Dissociation of Retinal Cells:*

The retina was dissected from the eyecup in Hanks' balanced salt solution (HBSS, pH 7.4), cut into pieces, and incubated in Ca^{2+}- and Mg^{2+}-free HBSS containing papain (40–45 U/ml, pH 7.4, Worthington, Lakewood, NJ) for 45 minutes at 37°C. The pieces of retina were transferred to medium containing Dulbecco's modified Eagle's medium (Invitrogen, Carlsbad, CA), 10% fetal bovine serum (Invitrogen), 1X penicillin-streptomycin-glutamine (Invitrogen), and DNase I (100 U/ml, pH 7.4; Worthington, Lakewood, NJ), and gently triturated by a narrow opening glass pipette to obtain suspensions of isolated cells. Isolated cells were pipetted into 12-well cell culture plates; each well contains a single coverslip coated with concanavalin A (1 mg/ml; Sigma-Aldrich, St. Louis, MO). The cells were incubated for 1–3 hours at 37°C to adhere to the coverslips.

vii. Calcium Imaging:

To minimize light exposure, all calcium imaging studies were conducted in darkness. Single coverslips were placed on a glass slide between two strands of vacuum grease and incubated in 1-2 μM Fluo-4 (Invitrogen) for 7-8 minutes at room temperature. The slide was placed into a superfusion chamber and subsequently placed on a fixed stage upright microscope (LSM 5 Pascal; Zeiss). A single-pass, gravity-feed perfusion system delivered ACSF mammalian extracellular Ringer and test solutions to the chamber at 1.3 ml/min. Test solutions consisted of high $[K^+]$ ACSF mammalian extracellular Ringers and drugs. Drugs were titrated for optimal concentration including somatostatin-14 (100 nM-100 μM; H-1490, Bachem, Torrance, CA) and L-054,264 (1-10μM; 2444; TOCRIS Biosciences, Ellisville, MO). Cells and processes were viewed with a long-working distance, water immersion objective (Achroplan 40x, 0.95 NA; Zeiss). Specific band pass filters were used to achieve proper separation of signals (for single labeling, 543/560 LP, for double labeling, 488/505-530 BP, 543/560 LP). Confocal images were captured

as single scans for identifying RFP positive TH cells and process and time series for assessing changes in Fluo-4 fluorescent intensity. Digital images were acquired at a magnification zoom of 1.5x, and a resolution of 1024 x 1024 pixels. Confocal images were acquired at an optical thickness between 0.5 and 0.7 μm and ~1.0 Airy Units.

Recordings were made from TH::RFP processes labeled by calcium indicator, Fluo-4 (Invitrogen, Carlsbad, CA). To control for bleaching during the time series imaging of the cells, all peaks of high [K+] induced depolarization with or without drugs were normalized to their baseline values. TH::RFP processes were depolarized with 60 mM high [K+] for 30 seconds followed by perfusion with regular mammalian Ringers for three minutes. Following the second high [K+] induced depolarization, cells were perfused in regular mammalian Ringer's and the drug of interest for 30 seconds. Cells were then perfused in high [K+] and drug of interest for 30 seconds followed by a perfusion of regular mammalian Ringer's and the drug of interest for 30 seconds. Cells were subsequently re-exposed to regular mammalian Ringer's. Finally, after three minutes of perfusion in regular mammalian Ringer's, cells were depolarized with high [K+] to confirm their viability.

viii. Data Analysis:

Data obtained from time series were analyzed using Microsoft Excel 2010 (Redmond, WA). The fluorescent intensities from 2-3 regions of interest (ROI) were graphed and normalized to adjust for bleaching. Baseline was determined as an average of the fluorescent intensities before the peak. Peak was determined as the maximum fluorescent intensity between the beginning of the rising phase to end of the falling phase. The ratio in fluorescent intensity between the control peak with high [K+] stimulation and the experimental peak with high [K+] stimulation and drug was determined as (Peak 2-Base 2)/(Peak 1-Base 2). Results are an average 4-5 imaging experiments for each control and drug study. Each imaging experiment consists of 6-7 time series with 1-2 ROIs per a time series.

IV. Results

ii. TH::RFP retina: Expression of tyrosine hydroxylase

TH::RFP retinal transverse sections processed with immunohistochemistry using antibodies against TH and SRIF revealed a co-localized and co-fasciculated anatomical pattern, respectively. The TH::RFP transgenic mouse model expresses red fluorescent protein, which makes for easy visualization. As shown with co-localized immunoreactivity of anti-TH, the TH::RFP is expresses type 1 DA amacrine cells, their soma, and thick and thin processes (Figure 4.1). In the transverse TH::RFP retinal slices stained with anti-TH, all anti-TH cells were positively co-localized; however, some TH::RFP positive DA cells were not stained in anti-TH processed slices (data not shown). Based on previous studies by Gustincich et al., there is a class of DA amacrine cells that are expressed in the TH::RFP transgenic mouse line, known as type 2 DA amacrine cells, which do not express TH in tissues stained with TH antibodies. The reason behind the lack of anti-TH staining in type 2 DA amacrine cells is unknown, it suggests that there could be a misexpression in the mouse line.

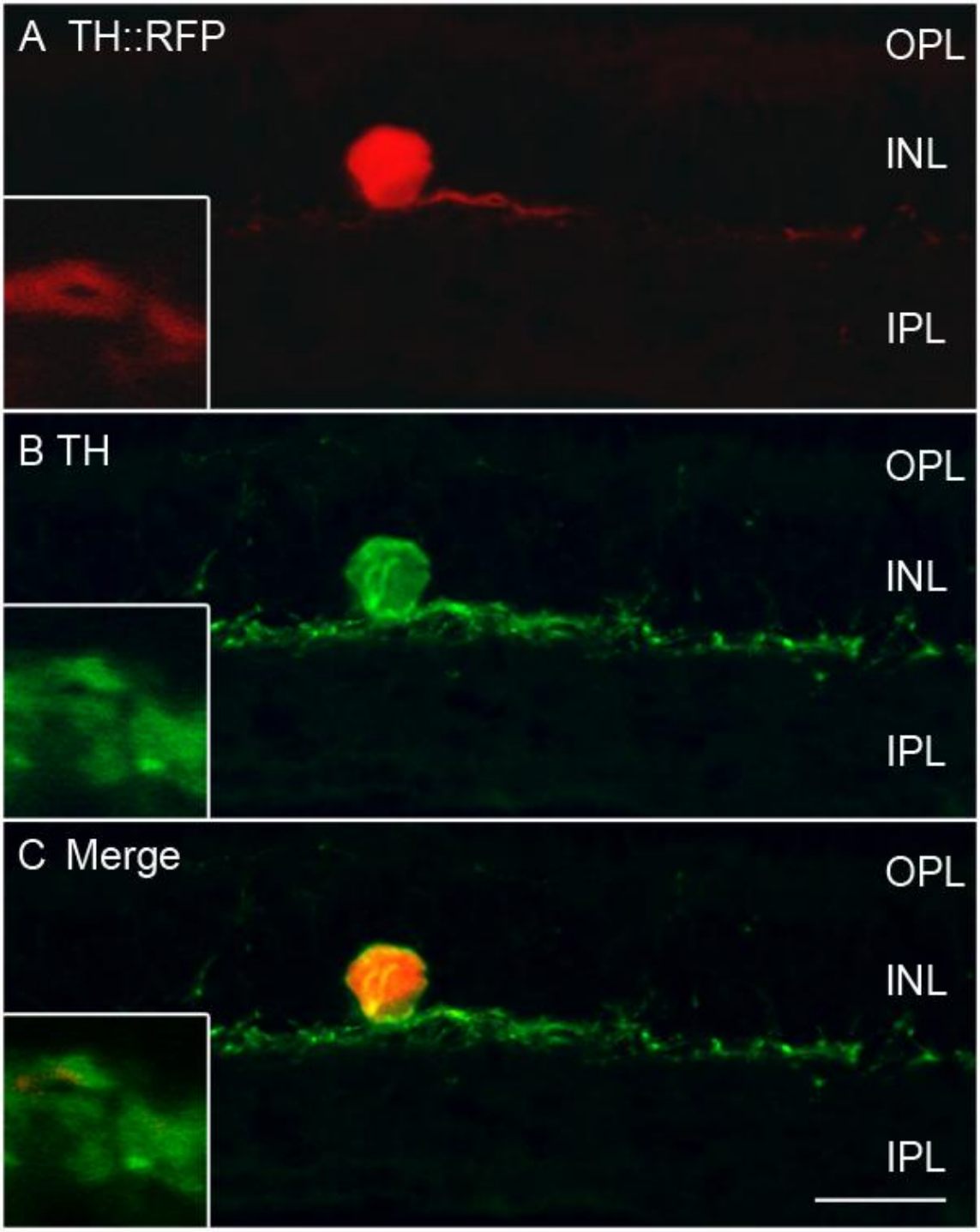

Figure 4.1. Specific expression of tyrosine hydroxylase in TH::RFP transgenic mouse retinal slices. (A) TH::RFP is robustly expressed in DA amacrine cells somas and proximal process. However, mores distal process are lightly labeled in comparison. (B) Anti-TH is robustly expressed in DA amacrine cell soma and processes located in the INL and sublamina 1 of the IPL, respectively. (C) Merged images of TH::RFP stained with anti-TH indicates the TH::RFP line positively expresses DA amacrine cells. Insets

are 4X zooms of proximal processes in the IPL that are anti-TH positive in the TH::RFP mouse line. Scale bar = 20 μM.

ii. TH::RFP retina: Expression of somatostatin

To confirm the presence of the unique co-fasiculatory pattern of TH- and SRIF-IR fibers in the TH::RFP transgenic mouse line, transverse retinal slices were stained with anti-SRIF. Our findings show the same close contact relationship between SRIF-IR fibers and TH::RFP-positive DA amacrine processes (Figure 4.2). The close contact relationship of SRIF-IR fibers and TH::RFP-positive DA amacrine cells is maintained throughout the IPL at both thick and thin DA amacrine cell processes. However, the same pattern is not clear in sublamina 3 of the IPL, or OPL. As shown in previous double labeled C57 Bl/6J retinal sections, SRIF-IR is not present in DA amacrine cells, and remain as two distinct amacrine cell subtypes.

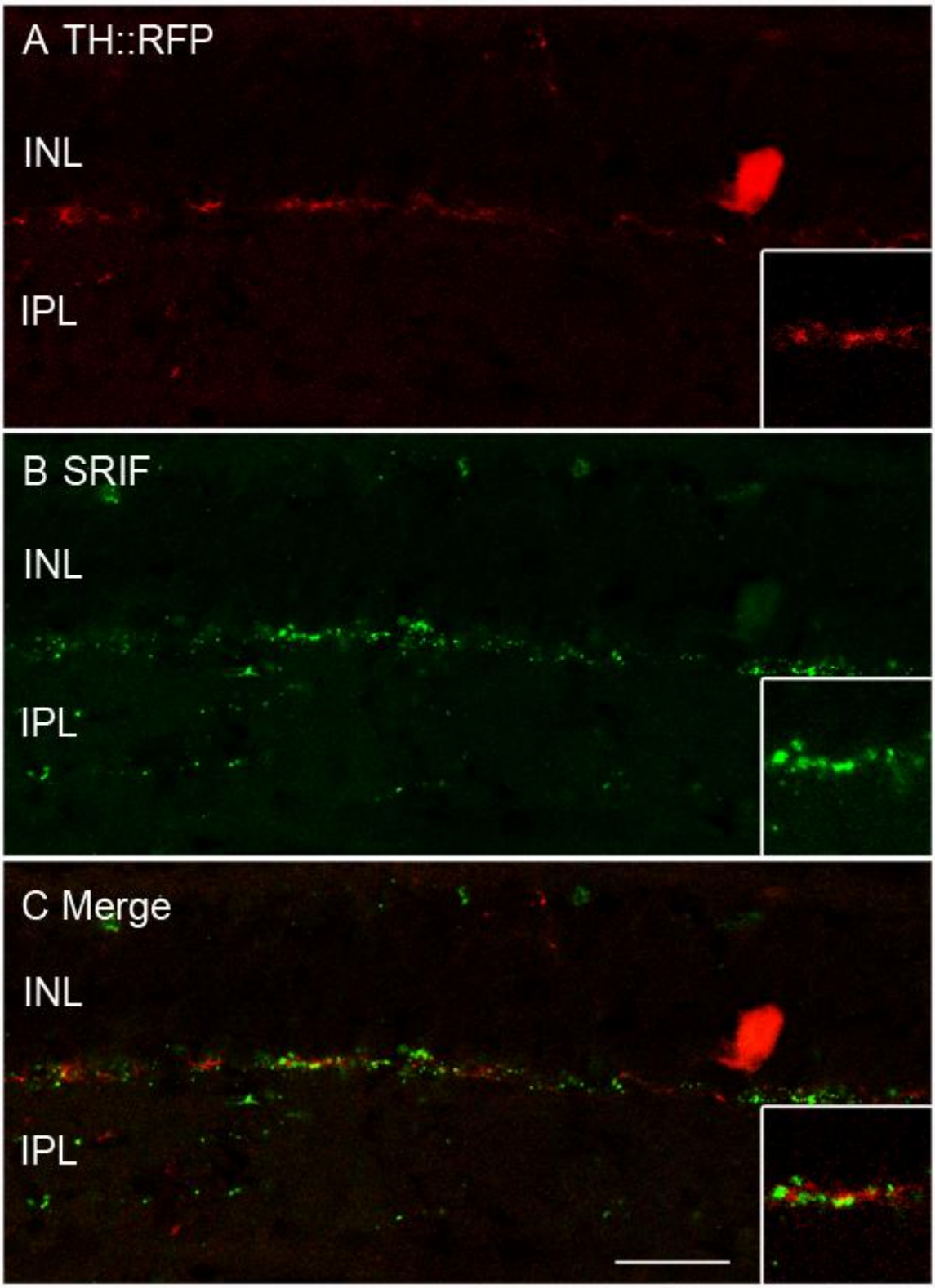

Figure 4.2. Pattern expression of SRIF in TH::RFP transgenic mouse retinal slices. (A) TH::RFP is robustly expressed in DA amacrine cells somas and proximal process. However, mores distal process are lightly labeled in comparison. (B) Puncta-like anti-SRIF processes are robustly expressed in sublamina 1,

3, and 5 of the IPL. (C) Merged images of TH::RFP stained with anti-SRIF indicates the TH::RFP line positively expresses the unique co-fasiculatory pattern between SRIF and DA amacrine cells. Insets are 4X zooms of close contact processes in the IPL in the TH::RFP mouse line. Scale bar = 20 μM.

In order to demonstrate functional significance to the described morphological pattern seen between TH-IR dopamine amacrine cells and SRIF-IR amacrine cells we had to utilize a transgenic mouse model that will allow for specific identification of dopaminergic amacrine cells in live preparations. Although the TH::RFP transgenic line is specific for labeling of dopaminergic amacrine cells, the yield of dopaminergic amacrine cell bodies is low, which makes it difficult for whole-cell patch clamping experiments. Hence, the creation of the TH::td-Tomato transgenic mouse model. The full characterization of the mouse line is currently being conducted in our laboratory. Preliminary results suggest that this mouse line is extremely non-specific. There are several cell types that are labeled, including: starburst amacrine cells, poly-axonal amacrine cells, ganglion cells, and dopamine amacrine cells.

iii. TH::td-Tomato retina: Expression of tyrosine hydroxylase

Identification of dopamine-containing amacrine cells using an antibody against tyrosine hydroxylase implicates the TH::td-Tomato transgenic mouse line as a worse model for the functional studies of dopaminergic amacrine cells. TH::td-tomato labels small-size (<10 μm) soma amacrine cells in the INL and some displaced in the GCL. Larger-size (>10 μm) somas were found to be either dopaminergic amacrine cells in the INL or ganglion cells in the GCL. TH::td-Tomato stratification in the IPL includes a thin band along sublamina 1 of the IPL and a relatively thicker band along sublamina 3 of the IPL. Interestingly, TH:td-Tomato clearly labels processes of the amacrine cells, whose dendrites extends from the soma in the INL, directly down to sublamina 3 of the IPL (Figure 4.3). Double labeling of TH::td-Tomato with anti-TH indicates not every dopaminergic amacrine cell is labeled, more specifically, only about 1 out 5 are labeled within a 200 μm x 200 μm area (Figure 4.4). However, immunolabeling with anti-TH only indicates that not every type 1 dopaminergic amacrine cell is labeled in the TH::td-Tomato

mouse model, this does not exclude the possibility that the type 2 dopaminerigc amacrine cell may be expressed. As described in previous studies, the type 1 dopaminergic amacrine cell is represented as a cell with a large and spherical soma and can be labeled using antibodies against TH; the type 2 dopaminergic amacrine cell has a small soma and does not show TH-IR. Both type 1 and type 2 dopaminergic amacrine cells are presented as interplexiform catecholaminergc amacrines in mammals (Versaux-Botteri et al., 1984, Mariani and Hokoc, 1988; Nguyen-Legors, 1988; Tauchi et al., 1990).

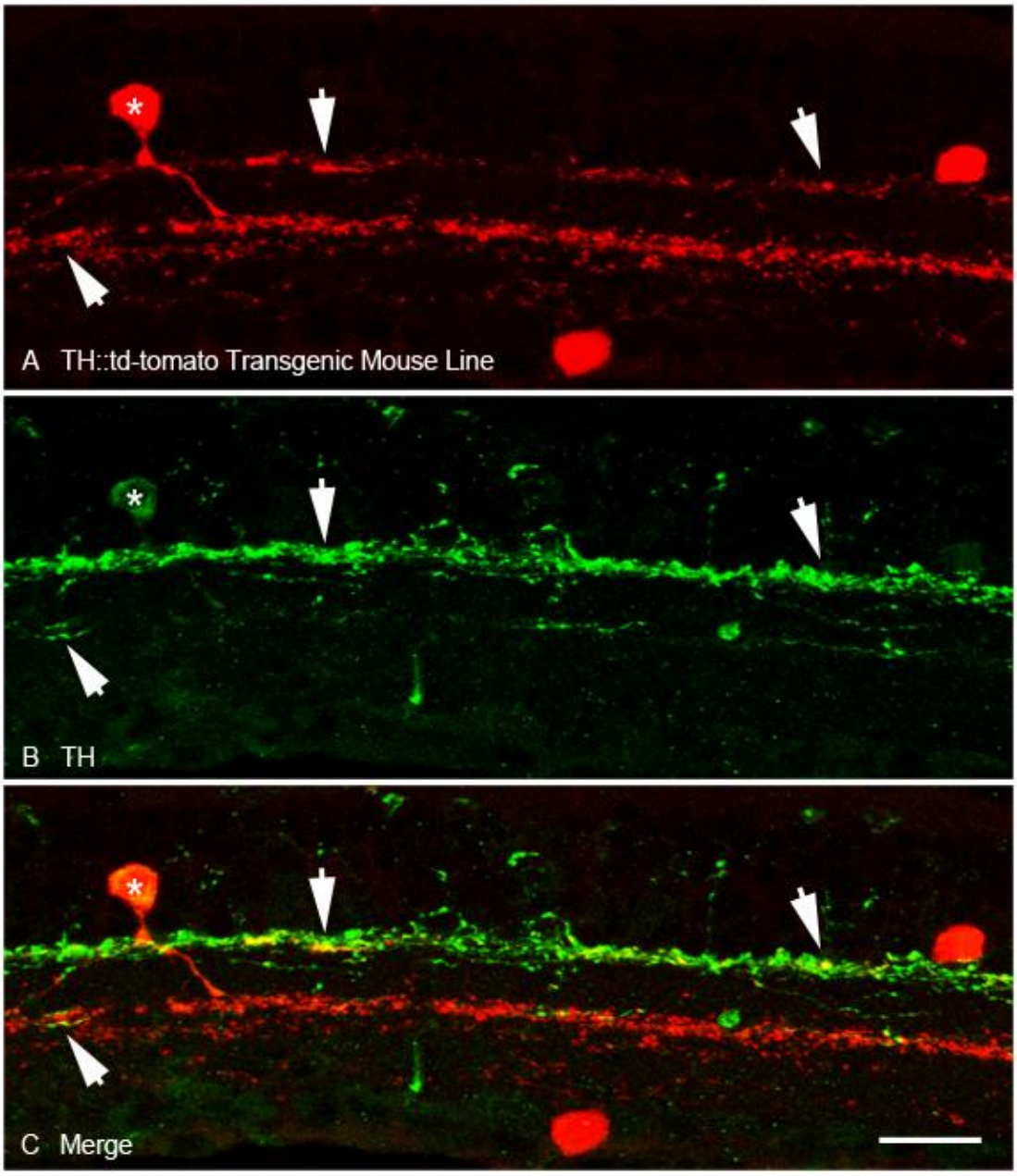

Figure 4.3. TH expression in TH::td-tomato transgenic mouse line. (A) TH::td-tomato transgenic mouse line labels small- to medium-sized cell somas in INL and GCL. Two bands of processes are labeled in lamina 1 (thin) and 3 (thick) of the IPL. (B) TH-IR extends throughout sublamina 1 (thick) and 3 (thin) of the IPL, as well as the occasional process that reaches out through the INL into the OPL. TH-IR cell somas are limited to the INL proximal to the IPL. (C) Merged images indicate not all cells labeled in the TH::td-Tomato transgenic mouse line are TH-IR. One out of three cells in this image co-localizes with TH immunolabeling, indicated by the asterisk. Not all processes labeled in the IPL are TH-IR. Arrows indicate specific localized co-immunoreactivity of TH with the transgenic mouse line. Scale bar = 20 µm. (Image courtesy of Michael Einstein)

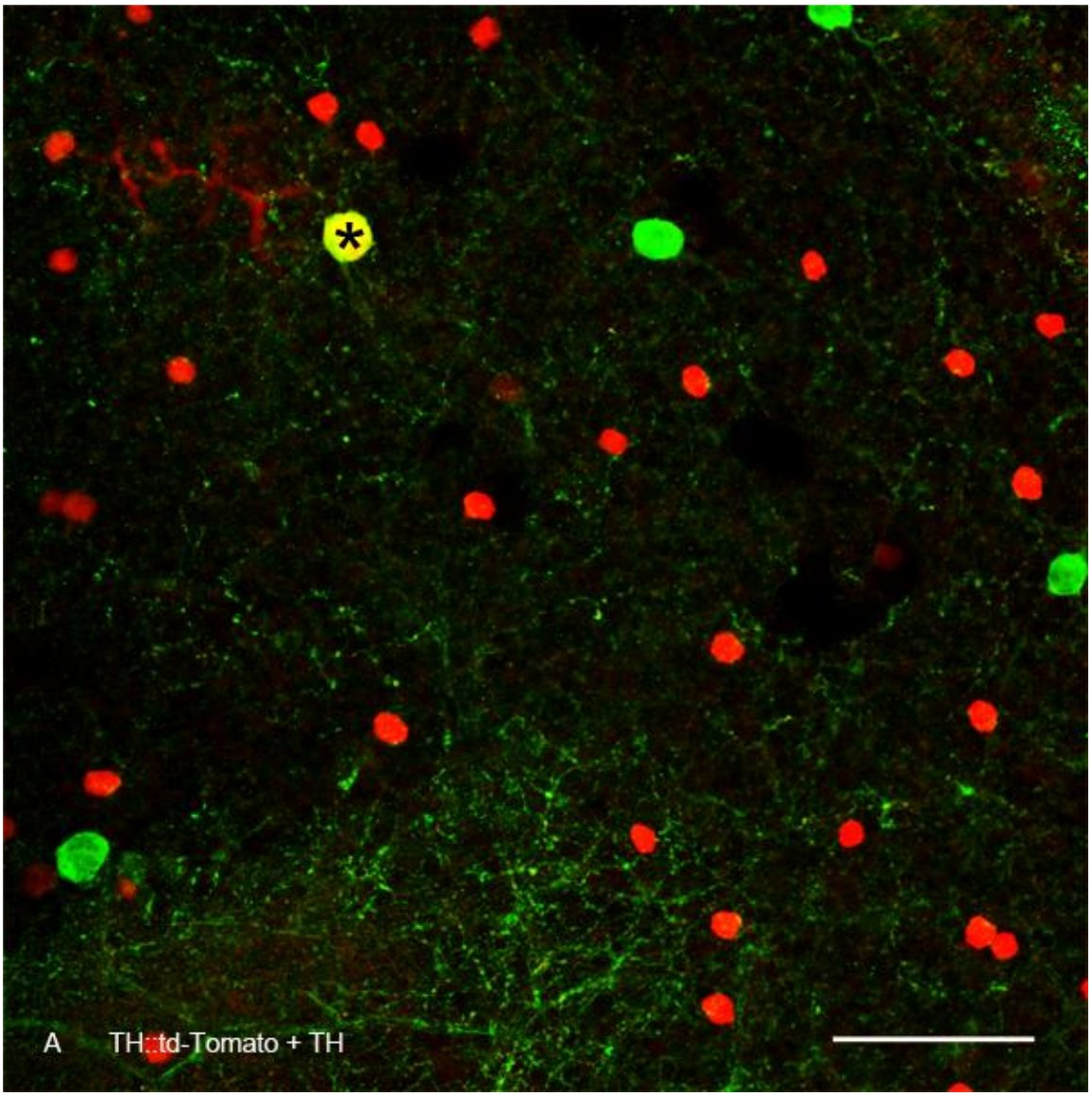

Figure 4.4. TH expression in TH::td-Tomato whole mount retina. (A) TH::td-tomato whole mount retina stained with TH shows 1 out of 5 labeled TH-IR cells are labeled in the transgenic mouse line. TH-IR processes are sparse and extend the entire retina. TH::td-tomato transgenic mouse line labels many small-sized cells not TH-IR. Asterisks denote TH-IR amacrine cell soma that is co-localized with a cell soma that is marked in this transgenic mouse line. Scale bar = 40 µm

iii. TH::td-Tomato retina: Expression of somatostatin

Even with its limitations the TH::td-Tomato mouse line could still offer an understanding to the functional interactions of between the morphological pattern seen between TH- and SRIF-IR fibers by doing single-cell RT-PCR, post-whole cell patch clamp recordings. However, in order to be sure that this

mouse line is sufficient for doing such experiments, we double labeled the TH::td-tomato transverse sections (Figure 4.5) and whole mount retinas (Figure 4.6) with antibodies against somatostatin. Results indicate these SRIF-IR process still form a co-fasciculatory pattern with putative dopaminergic amacrine cells in sublamina 1 of the IPL, as well as large putative dopaminergic somas. This pattern of SRIF-IR processes, localized to thick and thin varicose dopamine fibers, is not found on other cells in the same layer. Furthermore, no SRIF-IR cells are labeled in the TH::td-Tomato transgenic mouse model.

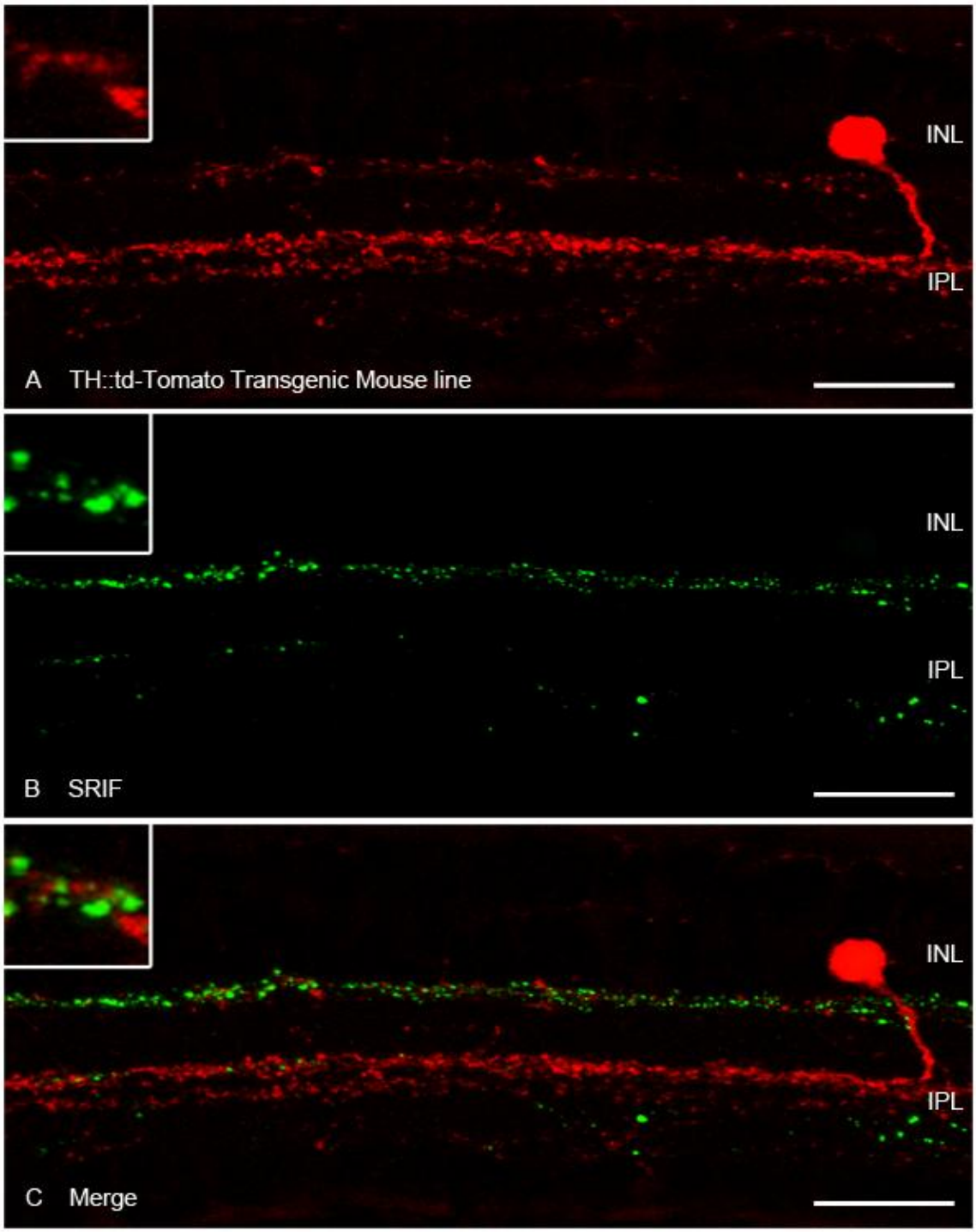

Figure 4.5. TH::td-tomato transgenic mouse line displays a similar pattern when stained with anti-SRIF (A) TH::td-tomato transgenic mouse line contains densely labeled processes in sublamina 3 of the IPL, and more sparsely in sublamina 1 of the IPL. Small-sized cell located in the INL, with a primary process that bypasses sublamina 1 and enters into sublamina 3 was also labeled. (B) Sparse SRIF punctate-like processes occupy sublamina 1, 3, and 5 of the IPL. (C) Merged image shows SRIF co-fasciculating with

processes of the transgenic mouse line in sublamina 1 and 3 of the IPL. Insets are 3X magnification of sublamina 1 processes that co-fasciculate. Scale bar = 20 µm.

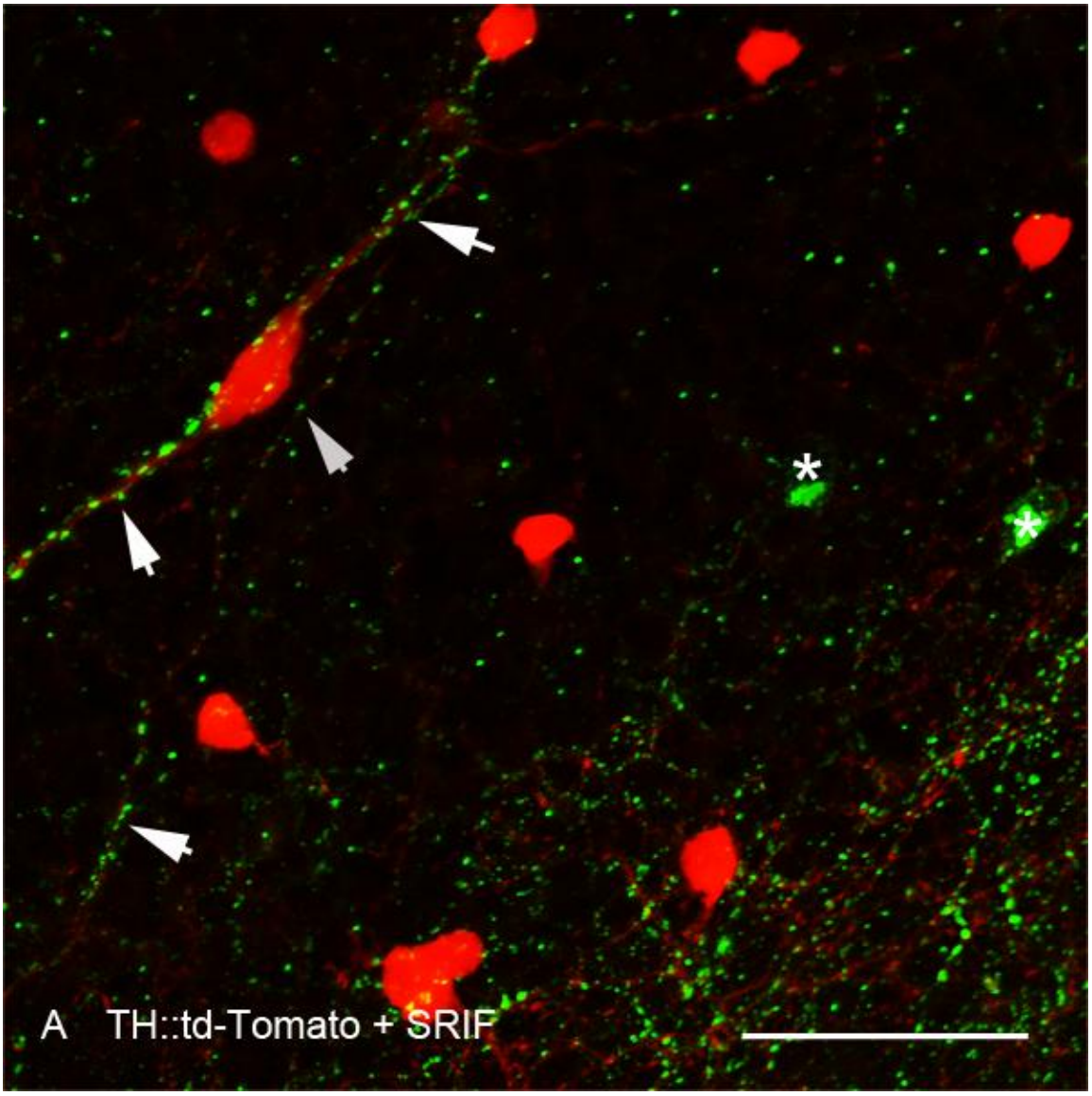

Figure 4.6. Whole mount TH::td-tomato retina stained with SRIF contain co-fasiculating patterns. (A) TH::td-tomato whole mount retina stained with anti-SRIF shows SRIF puncta-like processes running along putative dopaminergic amacrine cells. Arrows indicate examples of SRIF varicose processes encircling thick and thin varicose TH-processes. Asterisks denote SRIF amacrine cell somas, which do not co-localize with any cell somas marked in this transgenic mouse line. Scale bar = 40 µm

SRIF modulates TH::RFP amacrine cells: calcium imaging

To demonstrate the functional effects of SRIF and TH-IR contacts we utilized calcium imaging techniques and the TH::RFP transgenic line. With the use of Fluo-4 calcium indicator dyes we were able to examine the changes of intracellular calcium in isolated DA amacrine cell processes from TH::RFP retinas. Application of high extracellular K^+ solution (60 mM [K^+]) for 30 s produced a transient increase in intracellular Ca $^{2+}$ levels that declined with each subsequent high K^+ application. As shown in figure 4.7A, control consists of two high K^+ evoked Ca^{2+} transients, with a slight decrease in the second peak. With the application of SRIF (100 nM) during high K^+ application there was a significant decrease in intracellular Ca^{2+} levels compared to control ($P< 0.05$ vs control) (Figure 4.7B and 4.8). Cells were exposed to a third high K^+ stimulation to show viability of prep after application of drug (Figure 4.7B). In a dose response assay the different tested concentrations of SRIF did not show a significant change in effect on intracellular Ca^{2+} levels (Figure. 4.8). Previous studies using calcium imaging assays with SRIF suggest that the optimal SRIF concentration, taking into account half-life and binding affinity of the neuropeptide, is 1nM to 1µM (Johnson et al., 2001, Farrell et al., 2010).

To address how SRIF affects the intracellular Ca^{2+} of DA-amacrine cells we applied L-054,264 (sst_{2A} agonist) with the second application of high K^+. Mean data shows L-054,264 at 10 and 1 µM significantly decrease the levels of intracellular Ca^{2+} by 20 and 40%, respectively ($P<0.05$ vs control) (Figure 4.9). However, application of L-054,264 at 100 nM did not produce any significant decrease in transient intracellular Ca^{2+} levels.

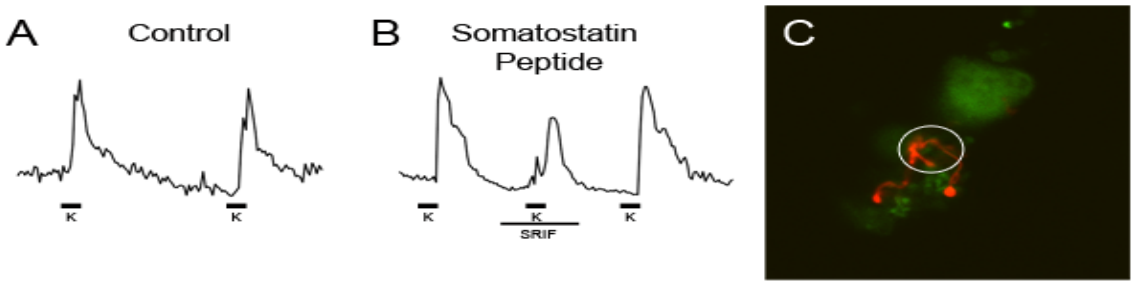

Figure 4.7. Intracellular Ca^{2+} signaling was reduced in the presence of SRIF. (A) Two applications of high K^+ for 30 s each time, produced two transient increases in intracellular Ca^{2+} levels. (B) Application of SRIF peptide (100 nM) with the second high K^+, produced a decrease in transient intracellular Ca^{2+} . The third high K^+ induced increase in intracellular Ca^{2+} demonstrates viability of cells post-application of drugs. (C) A fluorescent image of a TH::RFP-positive process in red (568nm stimulated) and fluo-4 (488nm stimulated). Circle indicates ROI used to make measurement of changes in fluorescent intensity.

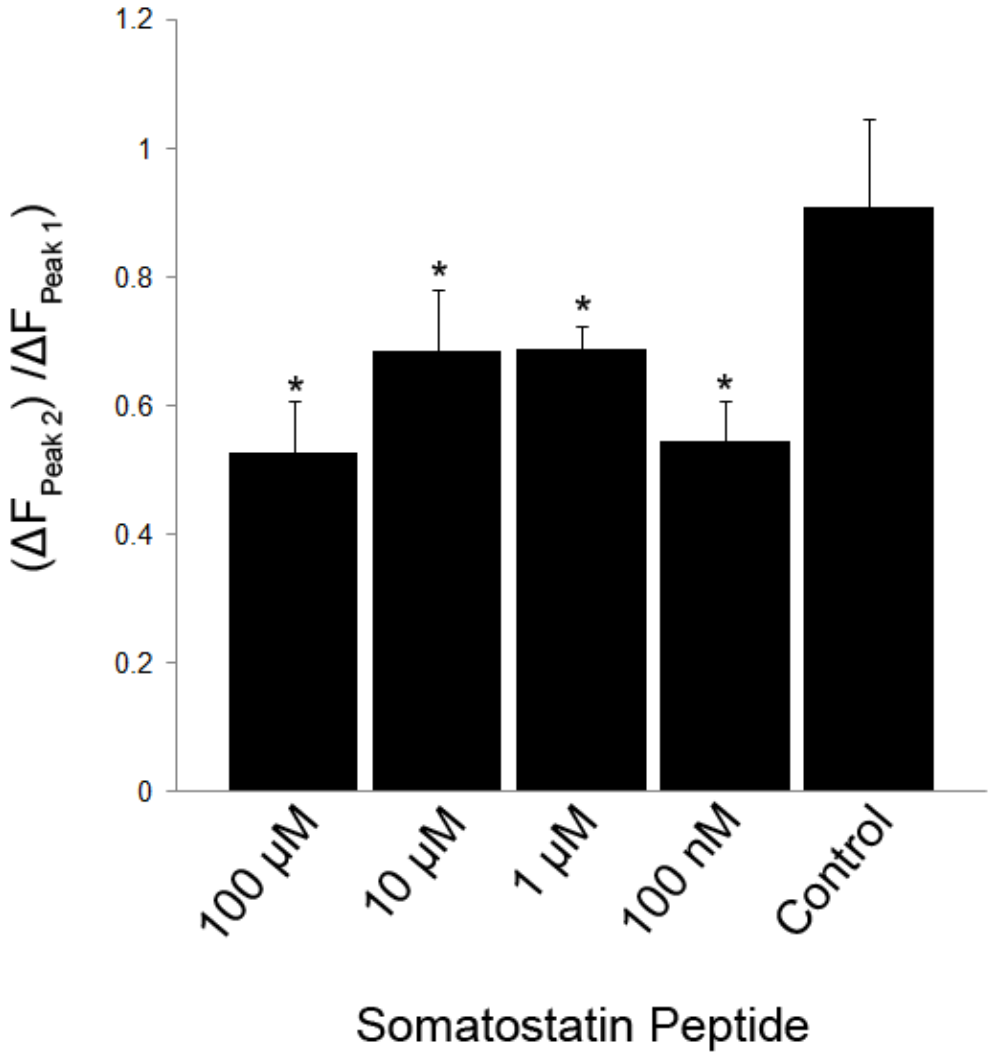

Figure 4.8. SRIF decreases intracellular Ca^{2+} signaling. Mean data show amplitudes of the second high K^+ response compared to the first high K^+ response. The mean Ca^{2+} transient amplitudes of all tested SRIF concentrations were significantly smaller than those of the control group, but did not show significant difference amongst themselves (n = 50 ROIs/concentration, 3-4 animals/concentration, *P<0.05, ANOVA)

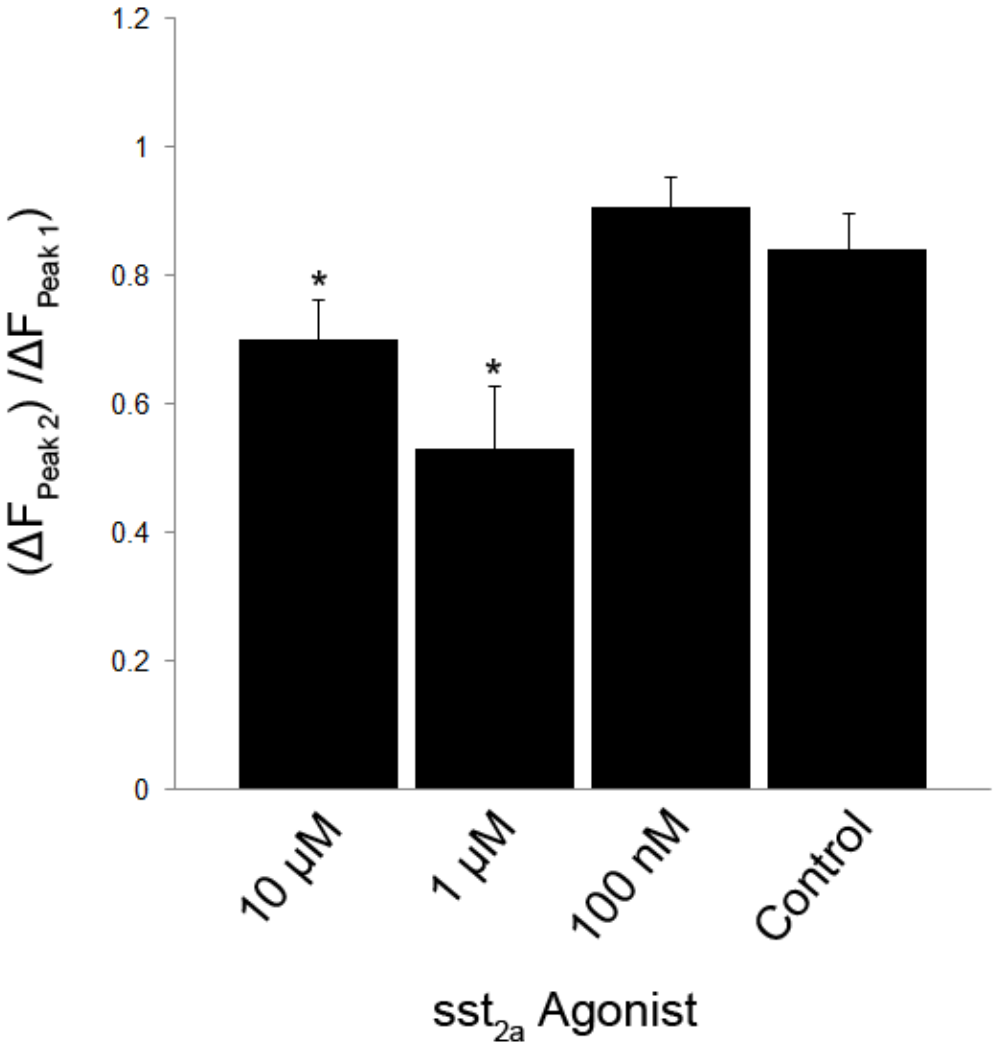

Figure 4.9. Sst_{2A} decreases intracellular Ca^{2+} signaling. Mean data show amplitudes of the second high K^+ response compared to the first high K^+ response. The mean Ca^{2+} transient amplitudes of L-054,264 (sst_{2A}

agonist) at 10 and 1 μM concentrations were significantly smaller than those of the control group, but did not show significant difference at 100 nM (n = 50 ROIs/concentration, 3-4 animals/concentration, *P<0.05, ANOVA)

V. Discussion

Using the TH:RFP transgenic animal model, which labels DA amacrine cells, we show that SRIF can inhibit intracellular Ca^{2+} levels in DA amacrine cells, and potentially inhibit the neurotransmission of DA amacrine cells. Calcium imaging evidence suggest that SRIF acts on sst2A receptors to modulate the intracellular Ca^{2+} levels. However, L-054,264 (sst_{2A} agonist) alone does not replicate the same level of decrease in intracellular Ca^{2+} levels seen with application of SRIF (Figure 4.8 and 4.9). This suggests that SRIF may act on its other receptors to elicit the decrease in intracellular Ca^{2+}. Independent studies using immunohistochemistry have localized other sst receptor subtypes to DA amacrine cell, including sst_1 and sst_5, suggesting the additional decrease of intracellular Ca^{2+} seen with application of SRIF compared to L-054,264 could be a result of SRIF acting on sst_1 and sst_5.

Future experiments

Although we have made much progress in looking at the morphology and functional relationship between SRIF and DA amacrine cells, there are still many questions left unanswered. First off, with the application of CYN 154806 (1843; TOCRIS Biosciences, Ellisville, MO), an sst_{2a} antagonist, would we see a reversal effect of SRIF? Secondly, we need to examine whether the mechanism by which SRIF modulates DA amacrine cells is a Ca^{2+} dependent process, and by means of which calcium channels? Thirdly, is the reciprocal morphological relationship applicable to functional modulation, in other words how does dopamine and D1 receptor agonist/antagonist affect SRIF amacrine cell membrane excitability and its intracellular Ca^{2+} levels? Finally, what is the bigger picture of the relationship between these two cells; do they affect non-image forming vision and pupillary reflexes by modulating intrinsically photosensitive retinal ganglion cells (ipRGCs)? Or is there some therapeutic relevance, as SRIF is known to effectively

allievate some symptoms seen in diabetic retinopathy? The studies I have shown are a stepping stone and only the tip of the iceberg to understanding the complex and broad influences of these two wide-field amacrine cells.

References

Akopian, A., J. Johnson, et al. (2000). "Somatostatin modulates voltage-gated K(+) and Ca(2+) currents in rod and cone photoreceptors of the salamander retina." J Neurosci 20(3): 929-36.

Badea, T. C. and J. Nathans (2004). "Quantitative analysis of neuronal morphologies in the mouse retina visualized by using a genetically directed reporter." J Comp Neurol 480(4): 331-51.

Boulland, J. L., M. Jenstad, et al. (2009). "Vesicular glutamate and GABA transporters sort to distinct sets of vesicles in a population of presynaptic terminals." Cereb Cortex 19(1): 241-8.

Brandstatter, J. H., U. Greferath, et al. (1995). "Co-stratification of GABAA receptors with the directionally selective circuitry of the rat retina." Vis Neurosci 12(2): 345-58.

Brecha, N. C. (1992). "Expression of GABAA receptors in the vertebrate retina." Prog Brain Res 90: 3-28.

Brecha, N. C., C. W. Oyster, et al. (1984). "Identification and characterization of tyrosine hydroxylase immunoreactive amacrine cells." Invest Ophthalmol Vis Sci 25(1): 66-70.

Brunk, I., C. Blex, et al. (2006). "The first luminal domain of vesicular monoamine transporters mediates G-protein-dependent regulation of transmitter uptake." J Biol Chem 281(44): 33373-85.

Casini, G. and N. C. Brecha (1992). "Colocalization of vasoactive intestinal polypeptide and GABA immunoreactivities in a population of wide-field amacrine cells in the rabbit retina." Vis Neurosci 8(4): 373-8.

Catalani, E., D. Cervia, et al. (2007). "Changes in neuronal response to ischemia in retinas with genetic alterations of somatostatin receptor expression." Eur J Neurosci 25(5): 1447-59.

Cervia, D. and P. Bagnoli (2007). "An update on somatostatin receptor signaling in native systems and new insights on their pathophysiology." Pharmacol Ther 116(2): 322-41.

Cervia, D., G. Casini, et al. (2008). "Physiology and pathology of somatostatin in the mammalian retina: a current view." Mol Cell Endocrinol 286(1-2): 112-22.

Cervia, D., D. Martini, et al. (2008). "Modulation of the neuronal response to ischaemia by somatostatin analogues in wild-type and knock-out mouse retinas." J Neurochem 106(5): 2224-35.

Chaudhry, F. A., R. J. Reimer, et al. (1998). "The vesicular GABA transporter, VGAT, localizes to synaptic vesicles in sets of glycinergic as well as GABAergic neurons." J Neurosci 18(23): 9733-50.

Contini, M. and E. Raviola (2003). "GABAergic synapses made by a retinal dopaminergic neuron." Proc Natl Acad Sci U S A 100(3): 1358-63.

Cristiani, R., C. Petrucci, et al. (2002). "Somatostatin (SRIF) and SRIF receptors in the mouse retina." Brain Res 936(1-2): 1-14.

Dal Monte, M., C. Petrucci, et al. (2003). "Somatostatin inhibits potassium-evoked glutamate release by activation of the sst(2) somatostatin receptor in the mouse retina." Naunyn Schmiedebergs Arch Pharmacol 367(2): 188-92.

Dal Monte, M., C. Petrucci, et al. (2003). "Genetic deletion of somatostatin receptor 1 alters somatostatinergic transmission in the mouse retina." Neuropharmacology 45(8): 1080-92.

Derouiche, A. and E. Asan (1999). "The dopamine D2 receptor subfamily in rat retina: ultrastructural immunogold and in situ hybridization studies." Eur J Neurosci 11(4): 1391-402.

Dowling, J. E. and B. Ehinger (1978). "Synaptic organization of the dopaminergic neurons in the rabbit retina." J Comp Neurol 180(2): 203-20.

Doyle, S. E., W. E. McIvor, et al. (2002). "Circadian rhythmicity in dopamine content of mammalian retina: role of the photoreceptors." J Neurochem 83(1): 211-9.

Epelbaum, J., P. Dournaud, et al. (1994). "The neurobiology of somatostatin." Crit Rev Neurobiol 8(1-2): 25-44.

Guo, C., A. A. Hirano, et al. "Guinea pig horizontal cells express GABA, the GABA-synthesizing enzyme GAD 65, and the GABA vesicular transporter." J Comp Neurol 518(10): 1647-69.

Guo, C., S. L. Stella, Jr., et al. (2009). "Plasmalemmal and vesicular gamma-aminobutyric acid transporter expression in the developing mouse retina." J Comp Neurol 512(1): 6-26.

Hirano, A. A., J. H. Brandstatter, et al. "SNAP25 expression in mammalian retinal horizontal cells." J Comp Neurol 519(5): 972-88.

Hirasawa, H., M. Puopolo, et al. (2009). "Extrasynaptic release of GABA by retinal dopaminergic neurons." J Neurophysiol 102(1): 146-58.

Johnson, J., D. W. Rickman, et al. (2000). "Somatostatin and somatostatin subtype 2A expression in the mammalian retina." Microsc Res Tech 50(2): 103-11.

Johnson, J., N. Tian, et al. (2003). "Vesicular neurotransmitter transporter expression in developing postnatal rodent retina: GABA and glycine precede glutamate." J Neurosci 23(2): 518-29.

Johnson, J., H. Wong, et al. (1998). "Expression of the somatostatin subtype 2A receptor in the rabbit retina." J Comp Neurol 393(1): 93-101.

Johnson, J., V. Wu, et al. (1999). "Somatostatin receptor subtype 2A expression in the rat retina." Neuroscience 94(3): 675-83.

Khrestchatisky, M., A. J. MacLennan, et al. (1989). "A novel alpha subunit in rat brain GABAA receptors." Neuron 3(6): 745-53.

Kiagiadaki, F., E. Koulakis, et al. (2008). "Dopamine (D1) receptor activation and nitrinergic agents influence somatostatin levels in rat retina." Exp Eye Res 86(1): 18-24.

Kiagiadaki, F. and K. Thermos (2008). "Effect of intravitreal administration of somatostatin and sst2 analogs on AMPA-induced neurotoxicity in rat retina." Invest Ophthalmol Vis Sci 49(7): 3080-9.

Knop, G. C., A. Feigenspan, et al. "Inputs underlying the ON-OFF light responses of type 2 wide-field amacrine cells in TH::GFP mice." J Neurosci 31(13): 4780-91.

Koulen, P., M. Sassoe-Pognetto, et al. (1996). "Selective clustering of GABA(A) and glycine receptors in the mammalian retina." J Neurosci 16(6): 2127-40.

Kouvidi, E., Z. Papadopoulou-Daifoti, et al. (2006). "Somatostatin modulates dopamine release in rat retina." Neurosci Lett 391(3): 82-6.

Li, H. B., C. B. Watt, et al. (1990). "Double-label analyses of somatostatin's coexistence with enkephalin and gamma-aminobutyric acid in amacrine cells of the chicken retina." Brain Res 525(2): 304-9.

Lin, B. and R. H. Masland (2006). "Populations of wide-field amacrine cells in the mouse retina." J Comp Neurol 499(5): 797-809.

MacNeil, M. A. and R. H. Masland (1998). "Extreme diversity among amacrine cells: implications for function." Neuron 20(5): 971-82.

Majumdar, S., J. Weiss, et al. (2009). "Glycinergic input of widefield, displaced amacrine cells of the mouse retina." J Physiol 587(Pt 15): 3831-49.

Marazioti, A., C. Spyraki, et al. (2009). "GABA antagonists reverse the somatostatin dependent attenuation of rat locomotor activity." Neuropeptides 43(3): 207-12.

Marc, R. E. and W. Liu (2000). "Fundamental GABAergic amacrine cell circuitries in the retina: nested feedback, concatenated inhibition, and axosomatic synapses." J Comp Neurol 425(4): 560-82.

Masland, R. H. "Cell populations of the retina: the Proctor lecture." Invest Ophthalmol Vis Sci 52(7): 4581-91.

Mastrodimou, N., F. Kiagiadaki, et al. (2006). "Somatostatin receptors (sst2) regulate cGMP production in rat retina." Regul Pept 133(1-3): 41-6.

Mastrodimou, N. and K. Thermos (2004). "The somatostatin receptor (sst1) modulates the release of somatostatin in rat retina." Neurosci Lett 356(1): 13-6.

Mastrodimou, N., A. Vasilaki, et al. (2006). "Somatostatin receptors in wildtype and somatostatin deficient mice and their involvement in nitric oxide physiology in the retina." Neuropeptides 40(5): 365-73.

Matsushita, N., H. Okada, et al. (2002). "Dynamics of tyrosine hydroxylase promoter activity during midbrain dopaminergic neuron development." J Neurochem 82(2): 295-304.

Miller, R. F. (2008). "Cell communication mechanisms in the vertebrate retina the proctor lecture." Invest Ophthalmol Vis Sci 49(12): 5184-98.

Momiyama, T. and L. Zaborszky (2006). "Somatostatin presynaptically inhibits both GABA and glutamate release onto rat basal forebrain cholinergic neurons." J Neurophysiol 96(2): 686-94.

Nguyen-Legros, J., C. Versaux-Botteri, et al. (1999). "Dopamine receptor localization in the mammalian retina." Mol Neurobiol 19(3): 181-204.

Olias, G., C. Viollet, et al. (2004). "Regulation and function of somatostatin receptors." J Neurochem 89(5): 1057-91.

Papadaki, T., M. Tsilimbaris, et al. "Somatostatin receptor activation (sst(1) -sst(5)) differentially influences human retinal pigment epithelium cell viability." Acta Ophthalmol 88(6): e228-33.

Pavan, B., S. Fiorini, et al. (2004). "Somatostatin coupling to adenylyl cyclase activity in the mouse retina." Naunyn Schmiedebergs Arch Pharmacol 370(2): 91-8.

Perez De Sevilla Muller, L., J. Shelley, et al. (2007). "Displaced amacrine cells of the mouse retina." J Comp Neurol 505(2): 177-89.

Peter, D., Y. Liu, et al. (1995). "Differential expression of two vesicular monoamine transporters." J Neurosci 15(9): 6179-88.

Pozdeyev, N., G. Tosini, et al. (2008). "Dopamine modulates diurnal and circadian rhythms of protein phosphorylation in photoreceptor cells of mouse retina." Eur J Neurosci 27(10): 2691-700.

Pozdeyev, N. V. and E. V. Lavrikova (2000). "Diurnal changes of tyrosine, dopamine, and dopamine metabolites content in the retina of rats maintained at different lighting conditions." J Mol Neurosci 15(1): 1-9.

Puopolo, M., S. E. Hochstetler, et al. (2001). "Extrasynaptic release of dopamine in a retinal neuron: activity dependence and transmitter modulation." Neuron 30(1): 211-25.

Reichlin, S. (1983). "Somatostatin." N Engl J Med 309(24): 1495-501.

Reichlin, S. (1983). "Somatostatin (second of two parts)." N Engl J Med 309(25): 1556-63.

Reisine, T. (1995). "Somatostatin." Cell Mol Neurobiol 15(6): 597-614.

Reisine, T. (1995). "Somatostatin receptors." Am J Physiol 269(6 Pt 1): G813-20.

Reisine, T. and G. I. Bell (1995). "Molecular biology of somatostatin receptors." Endocr Rev 16(4): 427-42.

Reisine, T. and G. I. Bell (1995). "Molecular properties of somatostatin receptors." Neuroscience 67(4): 777-90.

Rickman, D. W., J. C. Blanks, et al. (1996). "Somatostatin-immunoreactive neurons in the adult rabbit retina." J Comp Neurol 365(3): 491-503.

Sherry, D. M. and R. Heidelberger (2005). "Distribution of proteins associated with synaptic vesicle endocytosis in the mouse and goldfish retina." J Comp Neurol 484(4): 440-57.

Sherry, D. M., R. Mitchell, et al. (2006). "Distribution of plasma membrane-associated syntaxins 1 through 4 indicates distinct trafficking functions in the synaptic layers of the mouse retina." BMC Neurosci 7: 54.

Siehler, S., C. Nunn, et al. (2008). "Pharmacological profile of somatostatin and cortistatin receptors." Mol Cell Endocrinol 286(1-2): 26-34.

Thermos, K. (2003). "Functional mapping of somatostatin receptors in the retina: a review." Vision Res 43(17): 1805-15.

Tobin, A. J., M. Khrestchatisky, et al. (1991). "Structural, developmental and functional heterogeneity of rat GABAA receptors." Adv Exp Med Biol 287: 365-74.

van Hagen, P. M., G. S. Baarsma, et al. (2000). "Somatostatin and somatostatin receptors in retinal diseases." Eur J Endocrinol 143 Suppl 1: S43-51.

Vasilaki, A., Z. Georgoussi, et al. (2003). "Somatostatin receptors (sst2) are coupled to Go and modulate GTPase activity in the rabbit retina." J Neurochem 84(4): 625-32.

Vasilaki, A., M. Mouratidou, et al. (2002). "Somatostatin mediates nitric oxide production by activating sst(2) receptors in the rat retina." Neuropharmacology 43(5): 899-909.

Vasilaki, A. and K. Thermos (2009). "Somatostatin analogues as therapeutics in retinal disease." Pharmacol Ther 122(3): 324-33.

Veruki, M. L. and H. Wassle (1996). "Immunohistochemical localization of dopamine D1 receptors in rat retina." Eur J Neurosci 8(11): 2286-97.

Vugler, A. A., P. Redgrave, et al. (2007). "Dopamine neurones form a discrete plexus with melanopsin cells in normal and degenerating retina." Exp Neurol 205(1): 26-35.

Warrier, A., S. Borges, et al. (2005). "Calcium from internal stores triggers GABA release from retinal amacrine cells." J Neurophysiol 94(6): 4196-208.

Wassle, H., L. Heinze, et al. (2009). "Glycinergic transmission in the Mammalian retina." Front Mol Neurosci 2: 6.

Watt, C. B. and V. J. Florack (1993). "Double-label analyses of the coexistence of somatostatin with GABA and glycine in amacrine cells of the larval tiger salamander retina." Brain Res 617(1): 131-7.

White, C. A., L. M. Chalupa, et al. (1990). "Somatostatin-immunoreactive cells in the adult cat retina." J Comp Neurol 293(1): 134-50.

Witkovsky, P. (2004). "Dopamine and retinal function." Doc Ophthalmol 108(1): 17-40.

Witkovsky, P., B. Arango-Gonzalez, et al. (2005). "Rat retinal dopaminergic neurons: differential maturation of somatodendritic and axonal compartments." J Comp Neurol 481(4): 352-62.

Witkovsky, P., R. Gabriel, et al. (2000). "Influence of light and neural circuitry on tyrosine hydroxylase phosphorylation in the rat retina." J Chem Neuroanat 19(2): 105-16.

Witkovsky, P., R. Gabriel, et al. (2008). "Anatomical and neurochemical characterization of dopaminergic interplexiform processes in mouse and rat retinas." J Comp Neurol 510(2): 158-74.

Witkovsky, P., E. Veisenberger, et al. (2004). "Activity-dependent phosphorylation of tyrosine hydroxylase in dopaminergic neurons of the rat retina." J Neurosci 24(17): 4242-9.

Young, H. M. (1994). "Co-localization of GABA- and tyrosine hydroxylase-like immunoreactivities in amacrine cells of the rabbit retina." Vision Res 34(8): 995-9.

Zalutsky, R. A. and R. F. Miller (1990). "The physiology of somatostatin in the rabbit retina." J Neurosci 10(2): 383-93.

Zhang, D. Q., J. F. Stone, et al. (2004). "Characterization of genetically labeled catecholamine neurons in the mouse retina." Neuroreport 15(11): 1761-5.

Zhang, D. Q., K. Y. Wong, et al. (2008). "Intraretinal signaling by ganglion cell photoreceptors to dopaminergic amacrine neurons." Proc Natl Acad Sci U S A 105(37): 14181-6.

Zhang, D. Q., T. R. Zhou, et al. (2007). "Functional heterogeneity of retinal dopaminergic neurons underlying their multiple roles in vision." J Neurosci 27(3): 692-9.